Day-ahead stochastic scheduling of integrated electricity and heat system considering reserve provision by large-scale heat pumps

Zhang, Menglin; Wu, Qiuwei; Wen, Jinyu; Zhou, Bo; Guan, Qinyue; Tan, Jin; Lin, Zhongwei; Fang, Fang

Published in:
Applied Energy

Link to article, DOI:
10.1016/j.apenergy.2021.118143

Publication date:
2022

Document Version
Peer reviewed version

Applied Energy xxx (xxxx) xxx

Contents lists available at ScienceDirect

Applied Energy

journal homepage: www.elsevier.com/locate/apenergy

Day-ahead stochastic scheduling of integrated electricity and heat system considering reserve provision by large-scale heat pumps

Menglin Zhang [a], Qiuwei Wu [b,*], Jinyu Wen [c], Bo Zhou [c], Qinyue Guan [d], Jin Tan [b], Zhongwei Lin [e], Fang Fang [e]

[a] School of Automation, China University of Geosciences, Wuhan 430074, China
[b] Center for Electric Power and Energy (CEE), Department of Electrical Engineering, Technical University of Denmark (DTU), 2800 Kgs. Lyngby, Denmark
[c] State Key Laboratory of Advanced Electromagnetic Engineering and Technology, School of Electrical and Electronic Engineering, Huazhong University of Science and Technology, Wuhan 430074, China
[d] Economy and Technology Institute of State Grid Hubei Electric Power Company Limited, Wuhan 430077, China
[e] School of Control and Computer Engineering, North China Electric Power University, Beijing 102206, China

HIGHLIGHTS

- Explore benefits of using large-scale heat pumps to provide following and regulating reserves.
- Stochastic optimization of the integrated electricity and heat system co-optimizes energy, reserve, and heat regulation.
- Identify inactive transmission line constraints using an analytical calculation algorithm.

ARTICLE INFO

Keywords:
Large-scale heat pumps
Inactive constraint identification
Integrated electricity and heat system
Power-to-heat
Reserve provision
Stochastic optimization

ABSTRACT

Integrating power and heat sectors can increase the flexibility of wind power integration. Power-to-heat devices powered by renewables can promote the electrification and decarbonization of the heat sector. This paper explores the feasibility and benefits of using large-scale heat pumps for reserve provision. A two-stage stochastic optimization model is proposed for the day-ahead centralized scheduling of the integrated electricity and heat system considering wind power uncertainties, with reserve provision of large-scale heat pumps, combined heat and power units, and thermal power units. The model co-optimizes energy, following reserve, regulating reserve, and heat regulation to handle wind power uncertainties. To reduce the computational complexity of the scenario-based stochastic optimization problem, inactive transmission line constraints are identified and removed based on an analytical calculation method, which considers the influence of power consumption of large-scale heat pumps on the power flow of transmission lines. The benefits of using reserves from large-scale heat pumps are tested on the modified IEEE-118 bus integrated electricity and heat system. The simulation results show that using large-scale heat pumps to provide the following reserve and regulating reserve show similar impacts on saving cost and reducing wind energy curtailment, and the acceleration algorithm can save computation time by approximately 64%.

1. Introduction

1.1. Background and motivation

To mitigate climate change risks, the international community has pledged to limit global warming and achieve carbon neutrality [1]. An effective measure for achieving the goal is to replace fossil fuels with renewable energy sources (RES) [2]. Among the RES, wind power is one of the fastest-growing energy sources across the globe. For example, Denmark hit a major milestone in wind power production in 2020, supplying about 50.4% of its electricity consumption [3].

Integrating power and heat sectors is a promising way to increase the utilization of wind power [4]. In the integrated electricity and heat system (IEHS), power-to-heat (P2H) devices powered by renewables can promote the electrification and decarbonization of the heat sector [5].

* Corresponding author.
E-mail address: qw@elektro.dtu.dk (Q. Wu).

https://doi.org/10.1016/j.apenergy.2021.118143
Received 30 April 2021; Received in revised form 17 October 2021; Accepted 26 October 2021
Available online 19 November 2021

Nomenclature

Abbreviations

CHP	Combined heat and power
EPS	Electricity power system
HP	Heat pump
IEHS	Integrated electricity and heat system
MILP	Mixed-integer linear programming
P2H	Power-to-heat
RES	Renewable energy source
SP	Stochastic programming
ST	Thermal storage tank

Indices and sets

Ψ^{B}	Set of buses in the EPS
Ψ^{CHP}	Set of CHP units
Ψ^{HP}	Set of large-scale HPs
Ψ^{L}	Set of transmission lines
Ψ^{S}	Set of wind power scenarios
Ψ^{ST}	Set of thermal storage tanks
Ψ^{TU}	Set of thermal power units
Ψ^{W}	Set of wind farms
$\Theta^{TU/CHP/W/HP,d}$	Set of thermal units/CHP units/wind farms/HPs located on bus d
Φ^{Heat}	Set of buses with heat load
$\Omega^{CHP/HP/ST,d}$	Set of CHP units/HPs/STs on bus d
Λ^{T}	Set of time periods
Φ^{TU}	Set of linearized pieces of fuel cost curve of thermal power unit

Parameters

$C_i^{CHP/TU}$	Start-up cost of CHP unit/thermal power unit i
$C_i^{CHP/TU/HP,f\_up,cap}$	Capacity price of upward following reserve of CHP unit/thermal power unit/HP i
$C_i^{CHP/TU/HP,f\_dn,cap}$	Capacity price of downward following reserve of CHP unit/thermal power unit/HP i
$C_i^{TU/HP,r\_up,cap}$	Capacity price of upward regulating reserve of thermal power unit/HP i
$C_i^{TU/HP,r\_dn,cap}$	Capacity price of downward regulating reserve of thermal power unit/HP i
$C_i^{CHP/TU/HP,f\_up,dep}$	Price of deploying upward following reserve of CHP unit/thermal power unit/HP i
$C_i^{CHP/TU/HP,f\_dn,dep}$	Price of deploying downward following reserve of CHP unit/thermal power unit/HP i
$C_i^{TU/HP,r\_up,dep}$	Price of deploying upward regulating reserve of thermal power unit/HP i
$C_i^{TU/HP,r\_dn,dep}$	Price of deploying downward regulating reserve of thermal power unit/HP i
C^{LD}	Penalty price of load shedding
C^{W}	Penalty price of wind power curtailment
$D_i^{CHP/TU}$	Downward ramping rate of CHP unit/thermal power unit i
$f_i^{min,TU}$	Fuel cost of thermal power unit i when operating at the minimum power output
$f_i^{CHP,\ j}$	Power and heat production cost of vertex j in the operational region of CHP unit i
f_l^{max}	Maximum power of transmission line l
$g_{d,l}^{TU/CHP/W/HP/B}$	Distribution factor of thermal power units/CHP units/wind farms/HPs/loads at bus d on line l
$\overline{H}_i^{ST}/\underline{H}_i^{ST}$	Maximum/minimum heat energy status of ST i
$\overline{h}_i^{ST}$	Maximum charging and discharging heat rate of ST i
$h_i^{CHP,\ j}$	Heat production of vertex j for CHP unit i
$K_{i,k}^{TU}$	The slope rate of linearized piece k of thermal power unit i
$L_{i,t}$	Day-ahead load forecast value of bus i in time period t
N_T	Total time periods
$\overline{P}_i^{CHP/TU}$	Maximum output of CHP unit/thermal power unit i
$\underline{P}_i^{CHP/TU}$	Minimum output of CHP unit/thermal power unit i
$\overline{P}_{i,k}^{TU}$	Maximum value of the kth linearized piece of thermal power unit i
$p_i^{CHP,\ j}$	Power production of vertex j for CHP unit i
$\overline{P}_i^{HP}$	Maximum power consumption of large-scale HP i
$\underline{P}_i^{HP}$	Minimum power consumption of large-scale HP i
p_s	Probability of scenario s
$R_t^{r\_up,total}$	Minimum requirements of upward regulating reserve capacity in time period t
$t_{st,i}^{TU/CHP}$	Minimum operating time periods after starting up thermal power unit/CHP unit i
$t_{dn,i}^{TU/CHP}$	Minimum off-line time periods after shutting down thermal power unit/CHP unit i
$U_i^{CHP/TU}$	Upward ramping rate of CHP unit/thermal power unit i
$W_{i,t}$	Day-ahead wind power forecast value of wind farm i in time period t
$W_{i,t,s}$	Real-time wind power scenario value of wind farm i in time period t
η_i^{HP}	Power to heat efficiency of HP i

Variables

f	Total operational cost
f_1	Day-ahead total operational cost
$f_1^{TU/CHP/HP}$	Day-ahead operational cost of thermal power units/CHP units/HPs.
$f_{2,s}$	Real-time total operational cost under scenario s
$f_{2,s}^{TU/CHP/HP/W/LD}$	Real-time operational cost of thermal power units/CHP units/HPs/wind curtailment/load shedding under scenario s
$f_{i,t}^{CHP}$	Power and heat production cost of CHP unit i in period t
$h_{i,t}^{CHP/HP}$	Heat production of CHP unit/HP i in period t
$h_{i,t}^{ST}$	Day-ahead heat charging and discharging rate of ST i in period t
$h_{i,t,s}^{ST}$	Real-time heat charging and discharging rate of ST i in period t in scenario s
$\Delta h_{i,t,s}^{CHP/HP,f\_up}$	Heat regulation of CHP unit/HP i related to the upward following reserve deployment in period t in scenario s
$\Delta h_{i,t,s}^{CHP/HP,f\_dn}$	Heat regulation of CHP unit/HP i related to the downward following reserve deployment in period t in scenario s
$\Delta h_{i,t,s}^{HP,r\_dn/r\_up}$	Heat regulation of CHP unit/HP i related to the downward/upward regulating reserve deployment in period t in scenario s
$H_{i,t}^{ST}$	Day-ahead heat energy storage status of ST i in period t
$H_{i,t,s}^{ST}$	Real-time heat energy storage status of ST i in period t in scenario s
$p_{i,t}^{CHP/TU}$	Power generation of CHP/thermal power unit i in period t
$p_{i,t}^{HP}$	Power consumption of HP i in period t
$p_{i,t,k}^{TU}$	Power generation of the kth linearized piece of thermal power unit i in period t
$r_{i,t,s}^{CHP/TU/HP,f\_up,cap}$	Upward following reserve capacity of CHP unit/

thermal power unit/HP i in period t in scenario s

$r_{i,t,s}^{\mathrm{CHP/TU/HP,f\_dn,cap}}$ Downward following reserve capacity of CHP unit/thermal power unit/HP i in period t in scenario s

$r_{i,t,s}^{\mathrm{TU/HP,r\_up,cap}}$ Upward regulating reserve capacity of thermal power unit/HP i in period t in scenario s

$r_{i,t,s}^{\mathrm{TU/HP,r\_dn,cap}}$ Downward regulating reserve capacity of thermal power unit/HP i in period t in scenario s

$\Delta r_{i,t,s}^{\mathrm{CHP/TU/HP,f\_up,dep}}$ Deployed upward following reserve from CHP unit/thermal power unit/HP i in period t in scenario s

$\Delta r_{i,t,s}^{\mathrm{CHP/TU/HP,f\_dn,dep}}$ Deployed downward following reserve from CHP unit/thermal power unit/HP i in period t in scenario s

$\Delta r_{i,t,s}^{\mathrm{TU/HP,r\_up,dep}}$ Deployed upward regulating reserve from thermal power unit/HP i in period t in scenario s

$\Delta r_{i,t,s}^{\mathrm{TU/HP,r\_dn,dep}}$ Deployed downward regulating reserve from thermal power unit/HP i in period t in scenario s

$\Delta w_{i,t}$ Day-ahead wind power curtailment of wind farm i in period t

$\Delta w_{i,t,s}$ Wind power curtailment of wind farm i in period t in scenario s

$\Delta L_{i,t,s}$ Load curtailment of bus i in period t in scenario s

$u_{i,t}^{\mathrm{CHP/TU}}$ Variable to indicate the startup of CHP unit/thermal power unit i

$v_{i,t}^{\mathrm{CHP/TU}}$ Variable to indicate the shutdown of CHP unit/thermal power unit i

$x_{i,t}^{\mathrm{CHP/TU/HP}}$ On-off status of CHP unit/thermal power unit/HP i in time period t

$\alpha_{i,t,j}$ The jth vertex coefficient of the operational region of CHP unit i in period t

$\Delta\alpha_{i,t,s,j}^{\mathrm{f\_up}}$ Coefficient regulation of vertex j when CHP unit i deploys upward following reserve in period t in scenario s

$\Delta\alpha_{i,t,s,j}^{\mathrm{f\_dn}}$ Coefficient regulation of vertex j when CHP unit i deploys downward following reserve in period t in scenario s

As a source of demand-side flexibility in power systems, P2H devices can contribute to reducing curtailment of surplus wind energy, reshaping load profile to coincide with renewable energy generation, and providing grid services for the power sector [6].

Among P2H devices, large-scale electric heat pumps (HPs) are an attractive option for offering exceptionally high efficiency [7]. Different from individual HPs installed on the consumer side, large-scale HPs mainly refer to those connected to a district heating system (DHS) for collective heat supply [8] and usually have a relatively larger heating power capacity that is between 0.2 MW and 10 MW in Denmark [9]. Currently, with the green climate and energy policies, large-scale HPs are given substantial political and financial support for the deployment in Nordic countries such as Sweden and Denmark [10,11].

Previous research on the day-ahead scheduling of the IEHS with HPs mainly considers the flexibility of HPs in energy scheduling. The role of large-scale HPs in providing frequency control ancillary services has not been considered. According to the experimental results of the demonstration project in the EnergyLab Nordhavn of Denmark [12], large-scale HPs are able to ramp up/down by 50% in less than 150 s [13]. The fast-ramping performance makes large-scale HPs available to provide multiple ancillary services, even for the regulating reserve which needs a short response time. However, the benefits of large-scale HPs to provide different types of reserves have not been fully explored in the day-ahead scheduling of the IEHS.

Another important aspect of the day-ahead scheduling of the renewable-based IEHS is to make decisions under wind power uncertainty. Robust optimization (RO) and stochastic programming (SP) are the two most popular techniques for handling uncertainties. RO describes the uncertainty parameter with an easy-to-obtain uncertainty set which stresses the boundary information of uncertainties [14] while SO depicts the uncertainties with a probability distribution. This difference further makes RO and SO differ in conservativeness and computational complexity. RO makes decisions based on the worst case of uncertainties. Although RO can avoid the high computational complexity, it suffers from conservative decisions. Compared with RO, SP can reduce conservativeness and obtain more cost-effective decisions. However, to guarantee the solution quality, the scenario-based SP problem needs to consider a sufficient number of scenarios and may face a huge computational burden [15].

This paper adopts SP to make decisions of the day-ahead scheduling for the IEHS with large-scale HPs and considers reducing the computational complexity by identifying and removing inactive transmission line constraints. In [16], a transmission line constraint is defined as inactive if it can be eliminated without changing the solution to the original optimization problem. Identifying and removing inactive transmission line constraints can greatly simplify the original optimization problems. According to the power flow calculation, the power flow on a transmission line is influenced by the net power injection of each bus. In conventional identification methods, the net power injection of each bus only considers the power ranges of generators and treats power load as invariable. However, when large-scale HPs with large power capacity are integrated, the load variation on a bus caused by providing reserves is not negligible, which will have an impact on the power flow of transmission lines. Currently, the traditional identification method is not suitable for the IEHS where P2H devices have an impact on the power flow of transmission lines.

With the above-mentioned gaps, this paper focuses on the day-ahead stochastic scheduling of the IEHS, which considers the reserve provision by large-scale HPs and reducing the computational complexity by identifying inactive transmission line constraints.

1.2. Literature review

The day-ahead scheduling of the IEHS uses the integrated energy flow model as the basis. A steady-state model of the energy flow for the district energy system is proposed in [17]. The steady-state model has been widely adopted in the day-ahead scheduling of the IEHS due to the suitable level of detail for operational purposes. Notably, when the IEHS is for the transmission level, only the heat balance of the heating networks is considered in the scheduling [18]. Refs. [19] and [20] improve the accuracy of the heating network model. In [19], a dynamic optimal energy flow model of the IEHS is established, and the finite difference method is used to linearize the partial differential equation constraint. A novel component-oriented modeling method for the district heating network is presented in [20], which considers the thermodynamics of fluids. However, such a model brings a high computational burden, and its application in day-ahead scheduling has not been explored.

Improving operational flexibility is an important aspect of the day-ahead scheduling of the IEHS, which can help improve energy efficiency and accommodate more renewables. Electric boilers [21] and thermal storage tanks (STs) [22] are utilized to reshape power and heat load profiles so as to increase wind power utilization in the unit commitment of the IEHS. In [23], the heat pipelines are used as heat storage media to increase the operational flexibility in the economic dispatch of the IEHS, but the renewable energy and unit commitment are not considered. Ref. [24] leverages the thermal inertia of buildings to increase operational flexibility in the scheduling of distribution systems. The studies in [21]-[24] are all based on centralized scheduling.

Ref. [25] proposes a scheduling strategy suitable for decentralized operation of power and heating sectors. However, the paradigm of decentralized operation may hinder the power sector from harvesting the flexibility of the heating side, incentive mechanisms inducing flexibility of the heating side need to be specially designed [26].

The above methods of improving flexibility are mainly for the energy scheduling of the IEHS, which neglect the optimization of reserves. In the IEHS, the operating reserve is the major source of flexibility to respond to power imbalances. Providing reasonable reserves is indispensable so that the operational plan of day-ahead scheduling can be adjusted to balance wind power uncertainties in real time. Ref. [27] categorizes and defines various types of operating reserves in North America and Europe. In this paper, two types of reserves, namely the following reserve and regulating reserve, are considered, which are both used for normal operating conditions. The following reserve also called manual reserve or tertiary control reserve in Europe is on a slower time scale than regulating reserve. It is defined as movements amending day-ahead operational schedules to correct an imbalance that will occur in the future [28]. In contrast, the regulating reserve, also called secondary control reserve in Europe, is activated in the balancing market [29]. It corrects the current imbalance from the total load or generation that differs from the forecasted condition within a period that has been scheduled by the shortest dispatch interval.

Compared with two-stage RO [30] and deep learning [31], two-stage SP is an effective technique that can coordinate the optimization of energy and reserve while considering wind power uncertainties [32]. Two-stage SP can help achieve the minimum expected operational cost and wind power curtailment. In addition, the two stages build the link from day-ahead scheduling to real-time operation.

Conventionally, the operating reserve mainly comes from controllable generators with fast ramping capability. With the increasing deployment of P2H devices, large-scale HPs become new potential suppliers of the operating reserve. Recently there has been an increasing research interest on the reserve provision by large-scale HPs. A dynamic model of large-scale HPs is proposed in [33], which shows that large-scale HPs can provide regulating reserve effectively. However, the dynamic model is applicable for single HP devices instead of incorporating large-scale HPs into the IEHS. Ref. [34] coordinates a large-scale HP and a fleet of electric vehicles to provide regulating reserves, but the modeling is from the perspective of the demand side service providers.

In contrast to [33] and [34], refs. [35–37] consider the flexibility of large-scale HPs in the day-ahead scheduling of the IEHS. Ref. [35] evaluates the economic value of HPs based on a two-stage SP operational strategy, but the flexibility of HPs is used to cope with uncertainties of heat demand and electricity prices instead of wind power uncertainties. Refs. [36] and [37] co-optimize the energy and following reserve capacity in the day-ahead scheduling of the IEHS based on a two-stage SP model and a RO model, respectively, which utilize the power regulation of conventional generators and HPs to accommodate day-ahead forecast uncertainties. However, the research in [35–37] only considers one type of reserve. In [38], two types of reserves are co-optimized with energy in the day-ahead scheduling of the IEHS, i.e., the following reserve for normal operating conditions and primary frequency response reserve for contingencies. In [39], both the following reserve and regulating reserve are deployed in the IEHS, but the scheduling is on the real-time scale.

For reducing the computational complexity of the scenario-based SP model, the existing research on the identification of inactive transmission line constraints mainly focuses on the power systems. A fast identification method of inactive transmission line constraints is proposed in [16]. On the basis of [16], some other research makes further extensions. Ref. [40] proposes an identification method of inactive constraints suitable for real-time markets with wind power uncertainty. Ref. [41] utilizes a greedy algorithm and bound tightening strategy to identify inactive constraints in the security-constrained unit commitment problem. Ref. [42] proposes an acceleration method for the inactive transmission line constraints identification that combines neighborhood search and improved relaxation inducement to reduce the computation time of the unit commitment.

Little research considers inactive constraints identification in the optimization of the IEHS. The P2H devices connected to the IEHS usually have a relatively large capacity. When the P2H devices change power consumption to provide flexibility, the power flow of some transmission lines may be influenced due to the large capacity of P2H devices. However, the traditional fast identification methods in [16] and [40–42] are not suitable for the IEHS with large-capacity P2H devices due to the different mathematical properties of the power balance constraint.

1.3. Statement of contributions

In summary, little work considers the following reserve and regulating reserve provision simultaneously by large-scale heat pumps and reducing the computational complexity through inactive constraints identification in the day-ahead scheduling of the IEHS. Compared to the existing work, the main contributions of this paper are as follows:

- Propose a day-ahead stochastic scheduling scheme for the IEHS, which co-optimizes the unit commitment, energy, following reserve, regulating reserve, and heat regulation to handle wind power uncertainties at two stages;
- Build a detailed reserve provision model to balance wind power uncertainties in the proposed scheduling scheme, where conventional power units and large-scale HPs are coordinated to provide reserves; and
- Propose an analytical identification method of inactive transmission line constraints to reduce the computational complexity of the SP problem, which considers the impact of power changes of P2H devices on the power flow of transmission lines.

1.4. Organization of the paper

The remaining part of this paper is organized as follows. Section 2 gives an overview of the day-ahead stochastic scheduling scheme of the IEHS with large-scale HPs. Section 3 builds a scenario-based two-stage SP mathematical model for the IEHS based on the proposed scheme. Section 4 introduces the inactive constraints identification method used to reduce the computational complexity of the SP problem. The simulation results on a modified IEEE-118 bus system are presented and analyzed in Section 5, followed by the conclusions in Section 6.

2. Overview of day-ahead stochastic scheduling of IEHS

2.1. IEHS with large-scale HPs

The structure of the IEHS with large-scale HPs is shown in Fig. 1, where the power and heat sectors are coupled by combined heat and power (CHP) units and large-scale HPs. CHP units produce power and heat simultaneously, while large-scale HPs consume power to produce

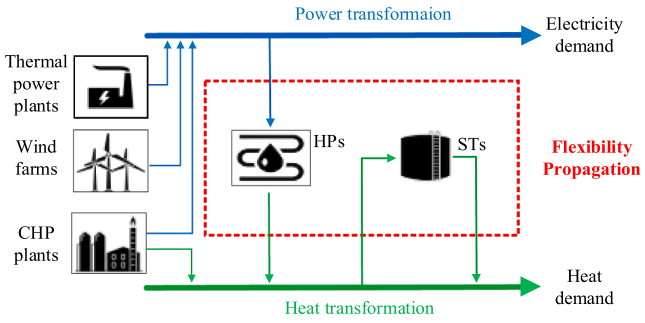

Fig. 1. Structure of the IEHS with large-scale HPs.

heat. In the power sector, the electricity load is also supplied by conventional thermal power units and wind power. In the heat sector, the STs are also integrated to increase the flexibility of heat regulation.

In the IEHS, thermal power generators and CHP units are the major sources for providing operating reserves. Large-scale HPs are treated as additional flexible devices for increasing operating reserve. The power imbalances in real-time caused by wind power uncertainty will be balanced by the combined delivery of the operating reserve from these resources.

2.2. Day-ahead stochastic scheduling scheme of IEHS

Similar to the electric power system (EPS), the IEHS needs to determine its operational plans at different stages, such as the day-ahead stage, intraday stage, and real-time stage, to gradually balance the production and consumption. The operators make decisions for each stage by including future uncertainties. In this paper, the intraday stage is not considered, and the day-ahead decisions are made with real-time uncertainties incorporated only. This is because the day-ahead scheduling and intraday scheduling handle future uncertainties with different strategies and time scales. In the day-ahead scheduling, the real-time uncertainties are represented and predicted on the basis of the day-ahead forecast, and the forecast span is a whole day. In contrast, intraday scheduling uses look-ahead dispatch to cope with uncertainties, and its forecasts are updated in a rolling-forward manner and the forecast span is usually several hours.

The day-ahead scheduling scheme based on two-stage SP is shown in Fig. 2. The proposed scheduling scheme utilizes two-stage SP to coordinate the optimization of energy and reserve while considering wind power uncertainties. The two stages refer to the day-ahead stage and real-time stage, and a link from day-ahead scheduling to real-time operation is built.

In the proposed scheme, the inputs are load and wind power predictions, as well as wind power uncertainty that is represented by a set of scenarios sampled from a known probability distribution. With the input, the IEHS operator minimizes the total operational cost including the day-ahead operational cost and expected real-time regulation cost. The optimization subjects to both the day-ahead operational constraints based on the day-ahead wind power forecast and real-time operational constraints under each uncertainty scenario of wind power. The day-ahead stage and real-time stage are coupled by the relationships between the reserve capacity and reserve deployment, as well as the relationship between heat production and heat regulation. The deployed reserve in real-time refers to the actually used reserve, which is conducted by activating the corresponding reserve capacity in the case of power imbalances. However, the amount of activation of each resource is allocated by real-time dispatch.

It should be noted that in the day-ahead scheduling of the IEHS, both the following reserve and regulating reserve capacity are considered. This is based on the further division of real-time operation, namely real-time prescheduling and real-time balancing [39]. The following reserve, which has a relatively slow delivery speed, is deployed in the real-time pre-scheduling stage to handle day-ahead forecast errors. In contrast, the regulating reserve, which has a faster delivery speed and less quantity demand, is deployed in the real-time balancing stage to deal with real-time forecast errors. In addition, heat regulation is necessary for real-time operation since the reserve provision of CHP units and large-scale HPs are closely related to their heat production.

The main objective of the day-ahead scheduling scheme is to obtain the optimal following reserve capacity, regulating reserve capacity, heat and power production plan, and unit commitment for devices in the IEHS. The following reserve capacity is provided by thermal power units, CHP units, and large-scale HPs, while the regulating reserve capacity is only allocated among thermal power units and large-scale HPs.

When the time comes to the real-time stage, the real-time scheduling will be executed by taking the day-ahead schedule and real-time forecast as inputs, which is out of the scope of this paper. Ref. [39] gives the details of real-time scheduling on the basis of this paper.

3. Mathematical formulation of day-ahead stochastic scheduling of IEHS

3.1. Coordination of energy, following reserve, and regulating reserve

In this subsection, large-scale HPs are taken as an example to illustrate how the energy scheduling, following reserve, and regulating reserve are coordinated.

Due to the fast response speed, large-scale HPs are able to provide not only the following reserve but also regulating reserve [13]. The increase and decrease of power consumptions of large-scale HPs are equivalent to the downward and upward reserve, respectively.

The reserve provision model of large-scale HPs is illustrated in Fig. 3. The original operational region of a large-scale HP is within $[\underline{P}^{HP}, \overline{P}^{HP}]$. In order to provide regulating reserve, its day-ahead operational region is limited within a smaller region $[\underline{P}^{HP} + r^{HP,r\_up,cap}, \overline{P}^{HP} - r^{HP,r\_dn,cap}]$. The day-ahead maximum power consumption is smaller than the actual upper boundaries $\overline{P}^{HP}$ to provide downward regulating reserve capacity $r^{HP,r\_dn,cap}$; the day-ahead minimum power consumption is greater than the actual lower boundaries $\underline{P}^{HP}$ to provide upward regulating reserve

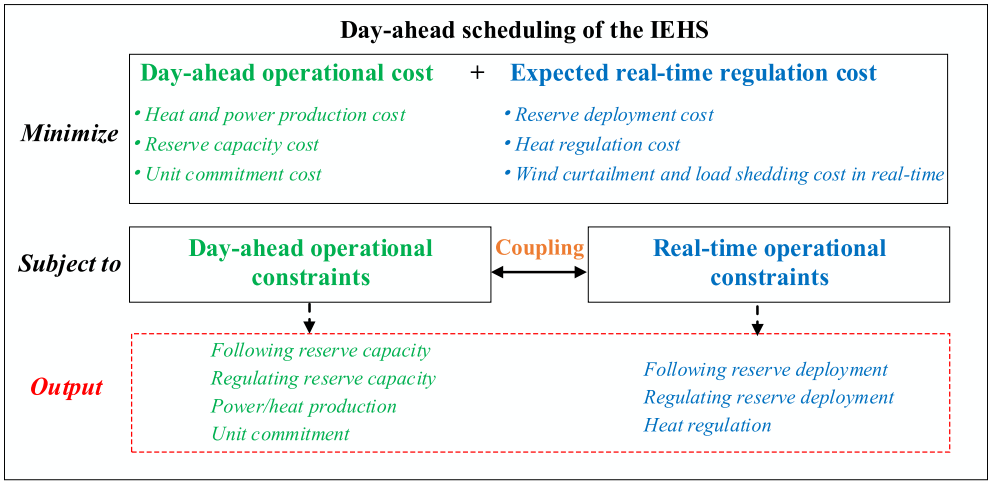

Fig. 2. Day-ahead stochastic scheduling scheme of the IEHS based on two-stage SP.

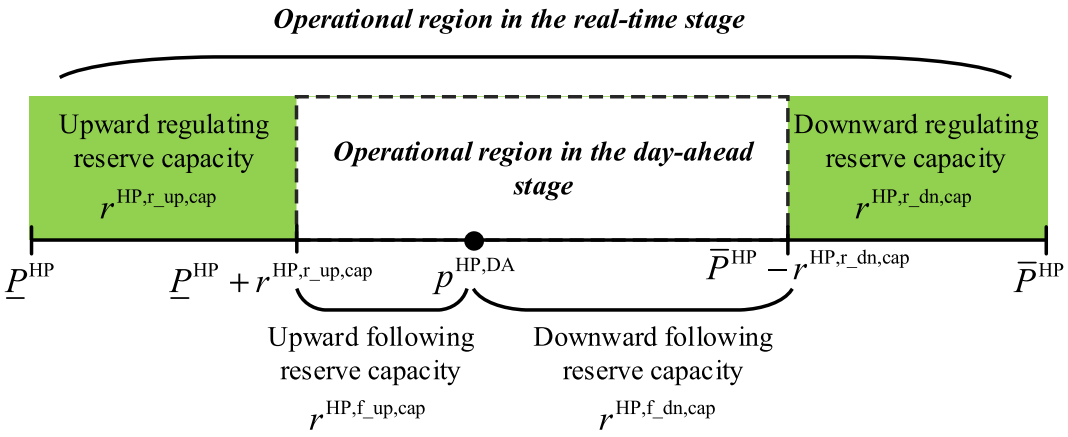

Fig. 3. Operational region of large-scale HPs for providing following and regulating reserves.

capacity $r^{HP,r\_up,cap}$. In contrast, the available following reserve capacity $r^{HP,f\_up,cap}$ and $r^{HP,f\_dn,cap}$ depends on the day-ahead schedule value $p^{HP,DA}$ and the day-ahead operational boundaries [$\underline{P}^{HP}$, $\overline{P}^{HP}$]. The detailed mathematical formulation of a large-scale HP providing following and regulating reserves is presented in (1).

$$\left(\underline{P}^{HP}+r^{HP,r\_up,cap}\right)\cdot x^{HP}\leqslant p^{HP,DA}\leqslant\left(\overline{P}^{HP}-r^{HP,r\_dn,cap}\right)\cdot x^{HP} \tag{1a}$$

$$r^{HP,r\_up,cap}=r^{HP,r\_dn,cap} \tag{1b}$$

$$r^{HP,f\_up,cap}\leqslant p^{HP,DA}-\left(\underline{P}^{HP}+r^{HP,r\_up,cap}\right)\cdot x^{HP} \tag{1c}$$

$$r^{HP,f\_dn,cap}\leqslant\left(\overline{P}^{HP}-r^{HP,r\_dn,cap}\right)\cdot x^{HP}-p^{HP,DA} \tag{1d}$$

$$p^{HP,pre}=p^{HP,DA}+r^{HP,f\_dn}-r^{HP,f\_up} \tag{1e}$$

$$p^{HP,bal}=p^{HP,pre}+r^{HP,r\_dn}-r^{HP,r\_up} \tag{1f}$$

$$0\leqslant\Delta r^{HP,r\_dn}\leqslant r^{HP,r\_dn,cap}\cdot x^{HP} \tag{1g}$$

$$0\leqslant\Delta r^{HP,r\_up}\leqslant r^{HP,r\_up,cap}\cdot x^{HP} \tag{1h}$$

$$0\leqslant\Delta r^{HP,f\_dn}\leqslant r^{HP,f\_dn,cap}\cdot x^{HP} \tag{1i}$$

$$0\leqslant\Delta r^{HP,f\_up}\leqslant r^{HP,f\_up,cap}\cdot x^{HP} \tag{1j}$$

where (1a) limits the day-ahead operational region of the power consumption of a large-scale HP with the on/off status x^{HP}; (1b) guarantees the upward and downward regulating reserves are symmetrical; (1c) and (1d) represent the available upward and downward following reserve capacity, respectively; (1e) models the transition of operational schedules of a large-scale HP from day-ahead scheduling to real-time prescheduling; (1f) models the transition of power consumption of a large-scale HP from real-time prescheduling to real-time balancing; (1g) and (1h) limit the activated maximum upward and downward regulating reserves, respectively; (1i) and (1j) limit the activated upward and downward following reserves. It should be noted that the ramping constraints of large-scale HPs are not considered due to their fast ramping speed.

3.2. Two-stage stochastic programming model of IEHS

The mathematical formulation of day-ahead stochastic scheduling based on two-stage SP is detailed in Appendix A. It co-optimizes the unit commitment, energy production plan, and reserve capacity in the day-ahead stage and the reserve deployment and heat regulation in the real-time stage to achieve minimum total cost and promote wind power integration.

The two-stage SP model in Appendix A is a mixed-integer linear programming (MILP) problem, the compact form of which is expressed as follows,

$$\begin{aligned} min\quad & f_1(\boldsymbol{x}_1)+\sum\nolimits_{s=1}^{S}\mathrm{p}_s\cdot f_{2,s}\left(\boldsymbol{y}_{2,s}\right) \\ s.t.\quad & \begin{cases} A_1\boldsymbol{x}_1\leqslant b_1 & (a) \\ A_2\boldsymbol{x}_1+B_2\boldsymbol{y}_{2,s}\leqslant b_{2,s},\forall s & (b) \end{cases} \end{aligned} \tag{2}$$

where $\boldsymbol{x}_1$ and $\boldsymbol{y}_{2,s}$ are day-ahead and real-time decision variables, respectively. (2a) represents day-ahead constraints in (A.2)-(A.8), and (2b) represents real-time constraints in (A.9)-(A.17).

4. Reducing computational complexity of SP model

As can be seen from (2), each scenario of real-time wind power outputs corresponds to a set of real-time constraints. When the number of scenarios increases, the optimization in (2) may face a heavy computational burden.

According to the fact that a large proportion of transmission line constraints are inactive in the power systems [16], identifying and removing inactive constraints in (2) can speed up the solution while having no influence on the decision results.

4.1. Inactive constraints identification theory

Theorem 1. ([16]:) *In an optimization problem with the feasible region* $\Omega=\{x\in R|Ax\leq b\}$, *the ith constraint* $A^ix\leq b^i$ *is inactive and can be removed from* Ω *if and only if* $\max_{x\in\Omega^{-i}}A^ix\leq b^i$, *where* Ω^{-i} *represents the feasible region after removing the ith constraint from* Ω .

For simplification, the upper limit of the transmission line constraint in (A.16) can be rewritten as follows,

$$\sum_{i\in\Theta^{TU,d}}\mathrm{g}_{d,l}^{TU}p_{i,t,s}^{TU}+\sum_{i\in\Theta^{CHP,d}}\mathrm{g}_{d,l}^{CHP}p_{i,t,s}^{CHP}+\sum_{i\in\Theta^{W,d}}\mathrm{g}_{d,l}^{W}\left(\mathrm{W}_{i,t,s}-\Delta w_{i,t,s}\right)-\sum_{i\in\Theta^{HP,d}}\mathrm{g}_{d,l}^{HP}p_{i,t,s}^{HP}-\sum_{i\in\Psi^{B}}\mathrm{g}_{d,l}^{B}\left(\mathrm{L}_{i,t}-\Delta L_{i,t,s}\right)\leqslant\mathrm{f}_l^{max} \tag{3}$$

where $p_{i,t,s}^{\mathrm{TU}}=p_{i,t}^{\mathrm{TU}}+\Delta r_{i,t,s}^{\mathrm{TU,f\_up,dep}}-\Delta r_{i,t,s}^{\mathrm{TU,f\_dn,dep}}+\Delta r_{i,t,s}^{\mathrm{TU,r\_up,dep}}-\Delta r_{i,t,s}^{\mathrm{TU,r\_dn,dep}}$, $p_{i,t,s}^{\mathrm{CHP}}=p_{i,t}^{\mathrm{CHP}}+\Delta r_{i,t,s}^{\mathrm{CHP,f.up,dep}}-\Delta r_{i,t,s}^{\mathrm{CHP,f.dn,dep}}$, and $p_{i,t,s}^{\mathrm{HP}}=p_{i,t}^{\mathrm{HP}}+\Delta r_{i,t,s}^{\mathrm{HP,f.dn,dep}}-\Delta r_{i,t,s}^{\mathrm{HP,f.up,dep}}+\Delta r_{i,t,s}^{\mathrm{HP,r.dn,dep}}-\Delta r_{i,t,s}^{\mathrm{HP,r.up,dep}}$.

In (3), $\Delta w_{i,t,s}$ and $\Delta L_{i,t,s}$ are slack variables of wind curtailment and load shedding to guarantee a nonempty feasible region. Since the non-zero values of these two set of variables can cause penalty cost, they are not expected in the optimization. In the identification of inactive transmission line constraints, the values of these two sets of slack variables are both set as zero.

According to Theorem 1, to determine whether (3) is an inactive constraint, we need to construct a maximization optimization problem, as described in (4), which takes the left hand of (3) as its objective, while subjecting to constraints set that removing (3) from the original feasible region in (2).

$$\max_{p_{i,t,s}^{\mathrm{TU}},p_{i,t,s}^{\mathrm{CHP}},p_{i,t,s}^{\mathrm{HP}},} \left\{ \sum_{i\in\Theta^{\mathrm{TU,d}}} g_{d,l}^{\mathrm{TU}} p_{i,t,s}^{\mathrm{TU}} + \sum_{i\in\Theta^{\mathrm{CHP,d}}} g_{d,l}^{\mathrm{CHP}} p_{i,t,s}^{\mathrm{CHP}} + \sum_{i\in\Theta^{\mathrm{W,d}}} g_{d,l}^{\mathrm{W}} W_{i,t,s} - \sum_{i\in\Psi^{\mathrm{B}}} g_{d,l}^{\mathrm{B}} L_{i,t} - \sum_{i\in\Theta^{\mathrm{HP,d}}} g_{d,l}^{\mathrm{HP}} p_{i,t,s}^{\mathrm{HP}} \right\} \tag{4}$$
$$s.t. \quad \text{Remove} \quad (3) \quad \text{from} \quad (2a) \cup (2b)$$

However, directly optimizing (4) is still time-consuming. In order to simplify the optimization, the following theorem can be utilized.

Theorem 2:. *Consider the LP problem in (5), which has the same objective as (4) but only considers the power balance constraints and the generation/consumption limit constraints of all devices.*

$$A_{l,t,s}^{+} = \max_{p_{i,t,s}^{\mathrm{TU}},p_{i,t,s}^{\mathrm{CHP}},p_{i,t,s}^{\mathrm{HP}},} \left\{ \sum_{i\in\Theta^{\mathrm{TU,d}}} g_{d,l}^{\mathrm{TU}} p_{i,t,s}^{\mathrm{TU}} + \sum_{i\in\Theta^{\mathrm{CHP,d}}} g_{d,l}^{\mathrm{CHP}} p_{i,t,s}^{\mathrm{CHP}} - \sum_{i\in\Theta^{\mathrm{HP,d}}} g_{d,l}^{\mathrm{HP}} p_{i,t,s}^{\mathrm{HP}} + \sum_{i\in\Theta^{\mathrm{W,d}}} g_{d,l}^{\mathrm{W}} W_{i,t,s} - \sum_{i\in\Psi^{\mathrm{B}}} g_{d,l}^{\mathrm{B}} L_{i,t} \right\}$$
$$s.t. \quad \begin{cases} \sum_{i\in\Psi^{\mathrm{TU}}} p_{i,t,s}^{\mathrm{TU}} + \sum_{i\in\Psi^{\mathrm{CHP}}} p_{i,t,s}^{\mathrm{CHP}} - \sum_{i\in\Psi^{\mathrm{HP}}} p_{i,t,s}^{\mathrm{HP}} + \sum_{i\in\Psi^{\mathrm{W}}} W_{i,t,s} = \sum_{i\in\Psi^{\mathrm{B}}} L_{i,t}, t\in\Lambda^{\mathrm{T}} \\ 0\leqslant p_{i,t,s}^{\mathrm{TU}} \leqslant \overline{P}_i^{\mathrm{TU}}, \\ 0\leqslant p_{i,t,s}^{\mathrm{CHP}} \leqslant \overline{P}_i^{\mathrm{CHP}} \\ 0\leqslant p_{i,t,s}^{\mathrm{HP}} \leqslant \overline{p}_i^{\mathrm{HP}} \end{cases} \tag{5}$$

Assuming that the optimal values of (4) and (5) are B_{lts}^{+} and A_{lts}^{+}, respectively, then it must hold for $B_{lts}^{+}\leq A_{lts}^{+}$. This is because the feasible region of (5) is a relaxation of (4). Therefore, if $A_{lts}^{+}\leq f_l^{\max}$, then $B_{lts}^{+}\leq f_l^{\max}$, and constraint (3) is inactive.

4.2. Analytical calculation for inactive constraints identification

Although (5) is an LP problem and it is much easier to be solved than (4), it still obtains the optimal value through optimization. In order to further speed up the identification, an analytical calculation method without optimization is proposed to determine whether (3) is inactive.

The optimization in (5) can be summarized as follows,

$$\max_{x,\ y} \quad z_1 = \sum_{i=1}^{N} a_i x_i + \sum_{i=1}^{M} b_i y_i + c$$
$$s.t. \begin{cases} x_1 + x_2 + \ldots + x_N - y_1 - y_2 - \ldots - y_M = h \\ 0\leqslant x_i \leqslant \overline{x}_i, \quad i = 1,2,\ldots,N \\ 0\leqslant y_i \leqslant \overline{y}_i, \quad i = 1,2,\ldots,M \end{cases} \tag{6}$$

where x represents the power generation of thermal power units and CHP units, y represents the power consumption of large-scale HPs, and c represents constant values of $\sum_{i\in\Theta^{\mathrm{W,d}}} g_{d,l}^{\mathrm{W}} W_{i,t,s} - \sum_{i\in\Psi^{\mathrm{B}}} g_{d,l}^{\mathrm{B}} L_{i,t}$.

It is worthwhile to note that in terms of mathematical properties, the optimization in (6) is different from the traditional identification problem in [16]. In the traditional identification problem, the power balance constraint only considers the outputs of generators. The traditional identification problem can be expressed as follows,

$$\max_{x,\ y} \quad z = \sum_{i=1}^{N} a_i x_i + c$$
$$s.t. \begin{cases} x_1 + x_2 + \ldots + x_N = h \\ 0\leqslant x_i \leqslant \overline{x}_i, \quad i = 1,2,\ldots,N \end{cases} \tag{7}$$

For the optimization in (7), the optimal value can be analytically determined by the coefficient ranking method without optimization [16], as shown in Fig. 4.

Firstly, sort the coefficients a_i $(i = 1, 2, \cdots, N)$ from largest to smallest. Let $i_1, i_2, \cdots, i_N$ be the permutation of 1, 2, …, N, such that $a_{i_1} \geq a_{i_2} \geq \cdots$

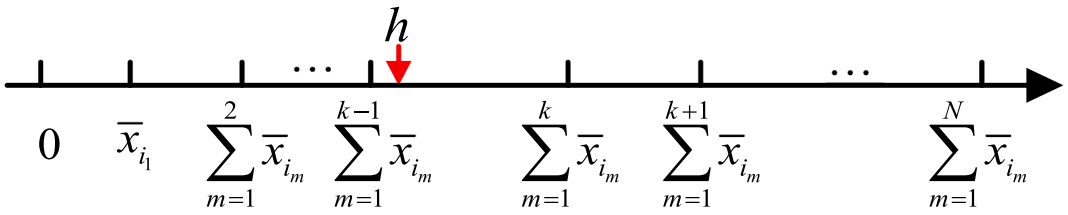

Fig. 4. Schematic diagram of coefficient ranking method.

$\geq a_{i_N}$. Secondly, find an integer k $(1 \leq k \leq N)$ to make $\sum_{m=1}^{k-1}\overline{x}_{i_m} \leqslant h \leqslant \sum_{m=1}^{k}\overline{x}_{i_m}$ satisfied, then the optimal solution can be calculated as (8), with the optimal value $a_{i_k}\left(h - \sum_{m=1}^{k-1} a_{i_m}\overline{x}_{i_m}\right) + \sum_{m=1}^{k-1} a_{i_m}\overline{x}_{i_m} + c$.

$$\begin{cases} x_{i_m} = \overline{x}_{i_m} & if \quad m \leqslant k-1 \\ x_{i_m} = h - \sum_{m=1}^{k-1}\overline{x}_{i_m} & if \quad m = k \\ 0 & if \quad m > k \end{cases} \tag{8}$$

However, due to the power consumption y of large-scale HPs in the power balance constraint, the coefficient ranking method cannot be directly used for the optimization in (6). According to the upper and lower limits of (6), the sum of $x_1 + x_2 + \cdots + x_N$ is within the range of $[h, h + \sum_{i=1}^{M}\overline{y}_i]$. Therefore, (6) can be transformed into the following form,

$$\begin{aligned} &\max_{x,\ y} \quad z_2 = \sum_{i=1}^{N} a_i x_i + \sum_{i=1}^{M} b_i y_i + c \\ &s.t. \begin{cases} h \leqslant x_1 + x_2 + \ldots + x_N \leqslant h + \sum_{i=1}^{M}\overline{y}_i \\ 0 \leqslant x_i \leqslant \overline{x}_i, \quad i = 1, 2, \ldots, N \\ 0 \leqslant y_i \leqslant \overline{y}_i, \quad i = 1, 2, \ldots, M \end{cases} \end{aligned} \tag{9}$$

In (9), x and y can be decoupled, that is, the optimization in (9) can be divided into two sub-problems related to x and y respectively, as shown in (10) and (11).

$$\begin{aligned} &\max_{y} \quad z_{21} = \sum_{i=1}^{M} b_i y_i \\ &s.t. \quad 0 \leqslant y_i \leqslant \overline{y}_i, \quad i = 1, 2, \ldots, M \end{aligned} \tag{10}$$

$$\begin{aligned} &\max_{x} \quad z_{22} = \sum_{i=1}^{N} a_i x_i \\ &s.t. \begin{cases} h \leqslant x_1 + x_2 + \ldots + x_N \leqslant h + \sum_{i=1}^{M}\overline{y}_i \\ 0 \leqslant x_i \leqslant \overline{x}_i, \quad i = 1, 2, \ldots, N \end{cases} \end{aligned} \tag{11}$$

For (10), there are only upper and lower limits for variable y. The optimal solution of z_{21} depends on the sign of b_i . If $b_i \leq 0$, then $y_i = 0$; otherwise, $y_i = \overline{y}_i$.

For (11), due to the introduction of large-scale HPs, the sum of $x_1 + x_2 + \cdots + x_N$ is within a range instead of being a constant as (7). The coefficient ranking method cannot be used directly. In such a case, the following method is proposed to analytically determine the optimal solution of (11).

Let h denotes any point within the range of $\left[h, h + \sum_{i=1}^{M}\overline{y}_i\right]$. Then for each possible power balance constraint $x_1 + x_2 + \cdots + x_N = h$, there is an optimization problem which is similar to (7) and can be analytically calculated by coefficient ranking method. Since each possible power balance constraint corresponds to an optimal value, the key to finding the maximum value of (11) is to find out candidate power balance constraints which may correspond to the optimization with maximum value.

Fig. 5 shows candidate points for power generation balance. By setting $h = h$ and $h = h + \sum_{i=1}^{M}\overline{y}_i$, two optimization problems in (12) and (13) can be obtained, respectively, which can be determined analytically by the coefficient ranking method. Assume that k_1 and k_2 are integers to make $\sum_{m=1}^{k_1-1}\overline{x}_{i_m} \leqslant h \leqslant \sum_{m=1}^{k_1}\overline{x}_{i_m}$ and $\sum_{m=1}^{k_2-1}\overline{x}_{i_m} \leqslant h + \sum_{i=1}^{M}\overline{y}_i \leqslant \sum_{m=1}^{k_2}\overline{x}_{i_m}$ satisfied, respectively. As can be seen from Fig. 5, apart from the two boundary points h and $h + \sum_{i=1}^{M}\overline{y}_i$, there are also candidate points $\left\{\sum_{m=1}^{k_1}\overline{x}_{i_m}, \ \ldots \ , \sum_{m=1}^{k_2-1}\overline{x}_{i_m}\right\}$ that may make the optimization have the maximum objective value, which correspond to integers from k_1 to $k_2 - 1$. This is because the kth $(k_1 \leq k \leq k_2 - 1)$ variable x_{i_k} will be either at zero or at its maximum value $\overline{x}_{i_k}$ to make the objective achieve its maximum value, depending on the sign of a_{i_k} .

$$\begin{aligned} &\max_{x} \quad z_{221} = \sum_{i=1}^{N} a_i x_i \\ &s.t. \begin{cases} x_1 + x_2 + \ldots + x_N = h \\ 0 \leqslant x_i \leqslant \overline{x}_i, \quad i = 1, 2, \ldots, N \end{cases} \end{aligned} \tag{12}$$

$$\begin{aligned} &\max_{x} \quad z_{222} = \sum_{i=1}^{N} a_i x_i \\ &s.t. \begin{cases} x_1 + x_2 + \ldots + x_N = h + \sum_{i=1}^{M}\overline{y}_i \\ 0 \leqslant x_i \leqslant \overline{x}_i, \quad i = 1, 2, \ldots, N \end{cases} \end{aligned} \tag{13}$$

Based on the candidate power balance points, the optimal value of z_{22} is calculated as follows,

$$z_{22} = max\left\{\begin{array}{l} a_{i_{k_1}}\left(h - \sum_{m=1}^{k_1-1} a_{i_m}\overline{x}_{i_m}\right) + \sum_{m=1}^{k_1-1} a_{i_m} x_{i_m}, \\ \ldots \\ \sum_{m=1}^{k} a_{i_m} x_{i_m}, \quad if \quad k_1 \leqslant k \leqslant k_2 - 1 \\ \ldots \\ a_{i_{k_2}}\left(h - \sum_{m=1}^{k_2-1} a_{i_m}\overline{x}_{i_m}\right) + \sum_{m=1}^{k_2-1} a_{i_m} x_{i_m} \end{array}\right\} \tag{14}$$

After the optimal objective values of z_{21} and z_{22} are determined, the optimal value of z_2 can be finally calculated as $z_2 = z_{21} + z_{22} + c$.

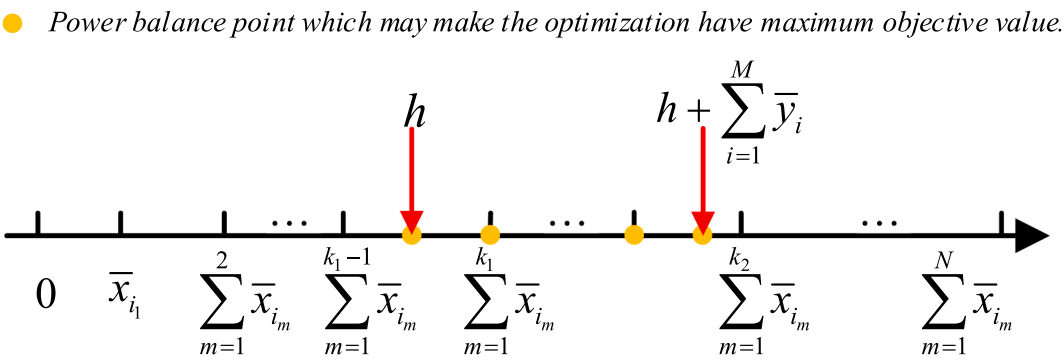

Fig. 5. Candidate power balance points that may make the optimization have maximum objective value.

Since the optimization of z_2 in (9) is a relaxation of the optimization of z_1 in (6), it must hold for $z_2 \geq z_1$. Therefore, if $z_2 \leq f_l^{max}$, then $z_1 \leq f_l^{max}$ and the lth transmission line constraint is inactive.

5. Case study

5.1. Test system description and case setting

The test system is modified from the IEEE-118 bus system to verify the performance of the proposed scheme, which includes 54 generators and 186 transmission lines. The reason of selecting this system is that it contains a large number of transmission lines and has computational difficulty when the scenario-based SP model is applied to this system. In reality, the energy consumption structure of an IEHS is different region by region, having different proportions of electricity and heat loads. In the modified test system, the energy consumption structure is set to be as similar as possible to a practical regional integrated energy system in the northeast part of China [36]. To ensure a similar energy consumption structure, parts of thermal power units in the test system are replaced with condensing CHP units, which are on buses 10, 18, 32, 49, 54, 56, 59, 61, 62, 80, 89, 99, and 104. Notably, each CHP unit is also integrated with a large-scale HP and an ST to jointly supply the heat demand.

The data for conventional generators and transmission networks are referred from [43]. The vertex coefficients data for condensing CHP units are referred from the Northeast Grid of China [36]. For each large-scale HP, the power capacity is 5 MW, and the coefficient of performance (COP) is 3. Six wind farms are connected to buses 25, 26, 65, 66, 87, and 100. Each wind farm has a capacity of 570 MW. The historical data of wind power used to generate wind power scenarios is from [44]. The day-ahead forecast profiles of power load, heat load, and wind power are given in Fig. 6.

In the optimization, the cost parameters are set as follows. The compensation for involuntary load shedding is 1000 $/MWh, which is usually set as a large value in different countries due to the possible losses to consumers [45]. The compensation for wind curtailment is set as 80 $/MWh, which is slightly above market price according to practices in Denmark [46]. The reserve capacity price of generators is priced at around 40% of their highest incremental price in [47]. Based on this, the costs of the following reserve capacity and regulating reserve capacity for conventional generators and CHP units are set at 40% of day-ahead maximum incremental cost and real-time maximum incremental cost, respectively. The energy price for reserve capacity actually used is set based on the two-price mechanism, for which the activation of upward reserves corresponds to a higher price than day-ahead energy price while the activation of downward reserves corresponds to a lower price

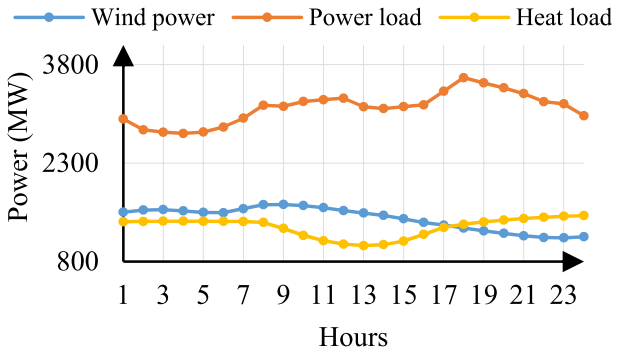

Fig. 6. Day-ahead forecast profiles of power load, heat load, and wind power.

than day-ahead energy price [48]. Therefore, the costs of deploying upward and downward following reserve of conventional generators and CHP units are set to 1.1 and 0.9 times of the day-ahead highest incremental cost of producing energy, respectively; while the cost of deploying upward and downward regulating reserve of conventional generators are set as 1.2 and 0.8 times of the real-time highest incremental cost of producing energy, respectively.

Table 1 lists five cases to compare the impact and effect of large-scale HPs on improving wind power utilization and reducing total operational cost when participating in energy scheduling and providing different types of reserves. In Table 1, FR and RR represent the following reserve and regulating reserve, respectively. The main difference among the five cases lies in the role of large-scale HPs. In Case 1.1, large-scale HPs are not considered. In Case 1.2, large-scale HPs only participate in the energy scheduling of the IEHS. In Case 1.3, large-scale HPs can participate in the energy scheduling and provide the following reserve. In Case 1.4, large-scale HPs can participate in the energy scheduling and provide the regulating reserve. In Case 1.5, the large-scale HPs can participate in the energy scheduling and provide both the following reserve and regulating reserves.

5.2. Performance analysis of large-scale HPs

In this section, the five cases in subsection 5.1 are simulated. The optimization problems are solved with GUROBI 9.1, and the tolerance gap is set to 0.05%.

Notably, large-scale HPs can be divided into different types such as sewage water source type, seawater sources type, and geothermal source type according to different heat sources. The heat sources may influence

Table 1
Case setting.

Cases	Thermal units			CHP units				Large-scale HP			ST
	Energy	FR	RR	Energy	FR	RR	Heat regulation	Energy	FR	RR	Heat regulation
Case 1.1	√	√	√	√	√	×	√	×	×	×	√
Case 1.2	√	√	√	√	√	×	√	√	×	×	√
Case 1.3	√	√	√	√	√	×	√	√	√	×	√
Case 1.4	√	√	√	√	√	×	√	√	×	√	√
Case 1.5	√	√	√	√	√	×	√	√	√	√	√

Table 2
Comparison of total operational costs and wind power curtailment in five cases

Cases	Day-ahead operational cost/$	Expected real-time operational cost/$	Total cost/$	Wind power curtailment rate	Percentage reduction of total cost
Case 1.1	1.882328×10^6	2.2542×10^5	2.107752×10^6	7.13%	–
Case 1.2	1.774328×10^6	1.0403×10^5	1.878357×10^6	2.64%	10.88%
Case 1.3	1.787364×10^6	8.2399×10^4	1.869763×10^6	2.61%	11.29%
Case 1.4	1.805319×10^6	7.9128×10^4	1.884448×10^6	2.27%	10.59%
Case 1.5	1.808864×10^6	7.2346×10^4	1.881210×10^6	2.34%	10.75%

the installation location, investment cost, and COP of large-scale HPs. Since this paper only focuses on the power consumption of HPs, the heat source type is not considered in this paper.

Table 2 compares the total operational cost and wind power utilization of five cases. In Table 2, percentage reduction of total cost of Cases 1.2, 1.3, 1.4, and 1.5 are calculated with Case 1.1 as the base. Compared with Case 1.1, the four other cases can significantly improve wind power utilization and cost savings.

As can be seen from the comparison of Cases 1.2, 1.3, 1.4, and 1.5, Case 1.2 has the lowest day-ahead operational cost. This is because in Case 1.2 the large-scale HPs only participate in the energy scheduling, the reserve capacity cost of large-scale HPs is saved. However, due to the less reserve capacity, Case 1.2 has a higher real-time operational cost, which is mainly caused by the larger reduction of wind power.

In contrast, Case 1.3 has the lowest total operational cost when HPs participate in the energy scheduling and provide following reserves. This is because the following reserve has a lower capacity price and deployment price than the regulating reserve. In Case 1.4, when HPs provide regulating reserve capacity, the energy scheduling of HPs will be limited in a smaller region, resulting in a higher day-ahead operational cost. But Case 1.4 has a lower real-time operational cost than Case 1.3 due to the fixed upward and downward regulating capability in real-time. Case 1.5 has the lowest real-time operational cost due to the larger flexibility for considering both following and regulating reserve. Besides, Case 1.5 is a compromise of Case 1.3 and Case 1.4 in wind power curtailment and total operational cost when HPs provide both the following reserve and regulating reserve.

The comparison results in Table 2 can be further explained by the operational plan and reserve deployment at different stages for the IEHS. The day-ahead scheduling and real-time operation are sequentially simulated to obtain the operational plan and the reserve deployment at different stages. Although the day-ahead stochastic scheduling of the IEHS co-optimizes the day-ahead and expected real-time operation costs, only the day-ahead operational plan is used. The actual real-time operation is based on the realization of wind power output in real-time. When it comes to the real-time stage, the real-time scheduling of the IEHS is executed by taking the day-ahead schedule as inputs. Ref. [39] details the real-time scheduling of the IEHS on the basis of this paper.

Fig. 7 shows the profiles of netload, the detailed operational plans of day-ahead scheduling, real-time prescheduling, and real-time balancing, and the deployment of following reserves and regulating reserves.

In Fig. 7 (a1), the net load is equal to the electricity demand minus wind power output. Fig. 7 (a) shows two obvious features. The first is that the netload of periods 1 to 8 is at a low level. The second is that in most time periods from 9 to 24, the day-ahead forecast of the net load is higher than the real-time forecast and real-time measurement, which means that the system needs to deploy downward reserves to achieve power balance.

According to Fig. 7 (b1) and (b2), when large-scale HPs are not considered, Case 1.1 has a large reduction of wind power in periods 1 to 8. This is mainly because the heat load during these periods is high, and the high generation outputs of CHP units limit the integration of wind power. In addition, in order to guarantee the required regulating reserve capacity, a few thermal power units are turned on to provide the regulating reserve, which also limits the integration of wind power.

In contrast, when the large-scale HPs participate in energy scheduling and provide reserves in Cases 1.2, 1.3, 1.4, and 1.5, the wind curtailment has been significantly reduced, as shown in Fig. 7 (c1)-(f2). The reasons are twofold. On the one hand, part of the redundant wind power is consumed by large-scale HPs. On the other hand, the power production of CHP units is reduced after using large-scale HPs to supply heat demands.

In Cases 1.2, 1.3, 1.4, and 1.5, the flexibility of large-scale HPs has different manifestations. In Case 1.2, HPs operate at the maximum power in all time periods when only participating in the energy scheduling, as shown in Fig. 7 (c1). In this case, the flexibility of HPs lies in changing the day-ahead operation of thermal power units and CHP units. In Case 1.3, instead of operating at maximum power in all periods, HPs reduce the power consumption in some periods to provide downward following reserve capacity in the day-ahead stage. In this case, the flexibility of HPs is embodied in the replacement of reserve of thermal power units in real-time prescheduling, as shown in Fig. 7 (d2). In Case 1.4, the flexibility of HPs is reflected in the less wind curtailment in the real-time balancing stage.

5.3. Performance of inactive transmission line constraint identification

Two cases are performed to validate the performance of the proposed

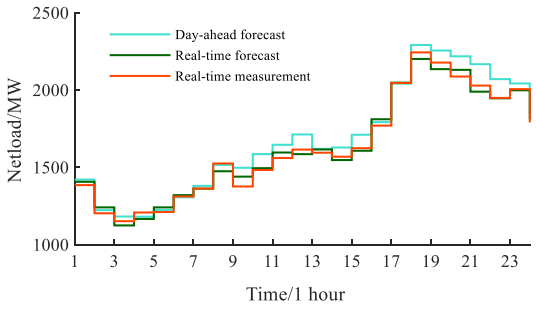

(a1) Netload profiles

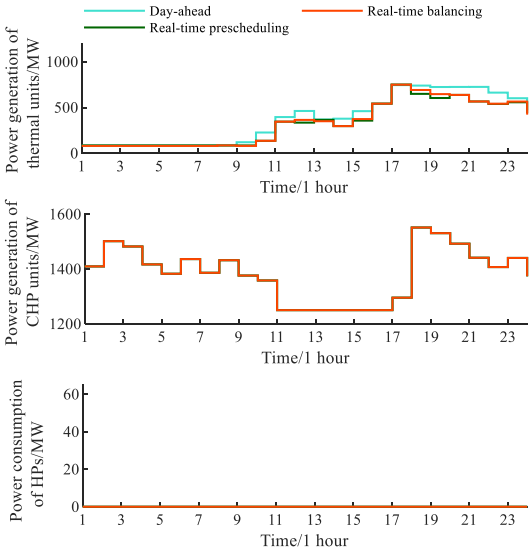

(b1) Operational plan of Case 1.1

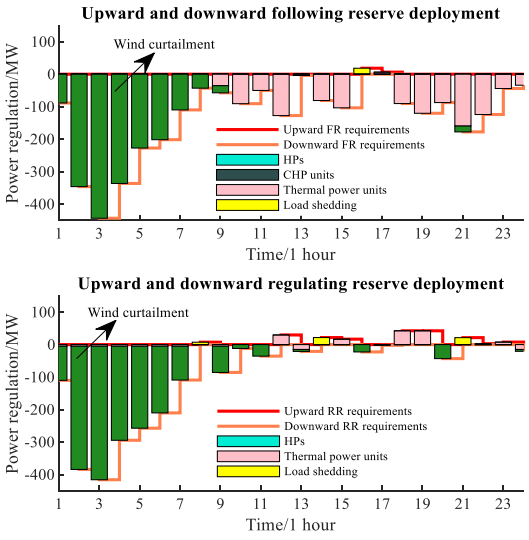

(b2) Reserve deployment of Case 1.1

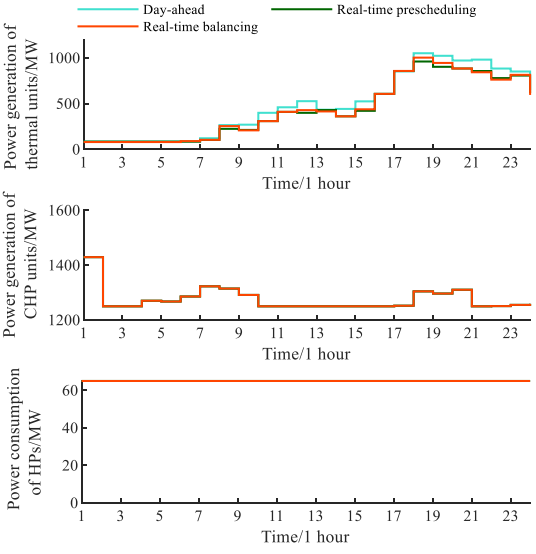

(c1) Operational plan of Case 1.2

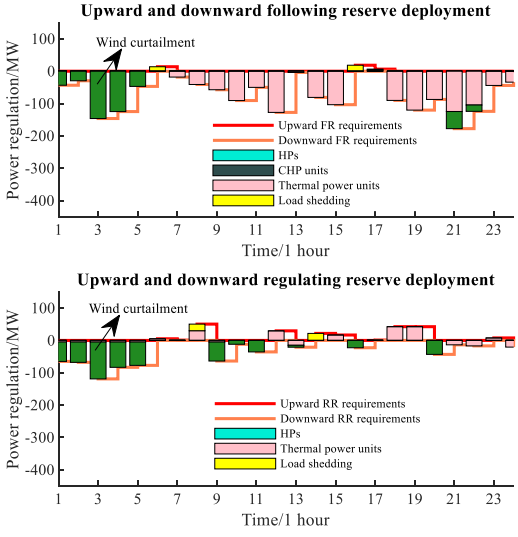

(c2) Reserve deployment of Case 1.2

Fig. 7. Operational plans and reserve deployment of the IEHS at different stages.

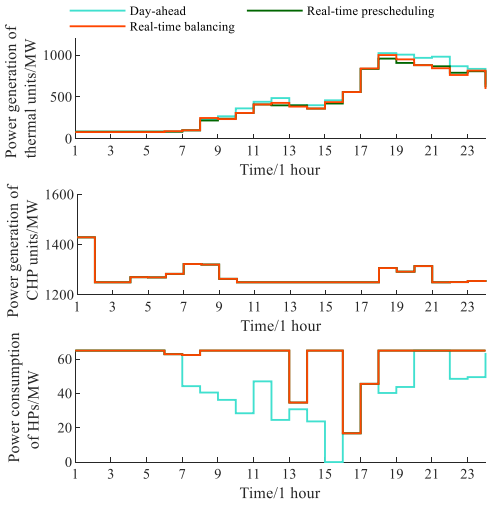

(d1) Operational plan of Case 1.3

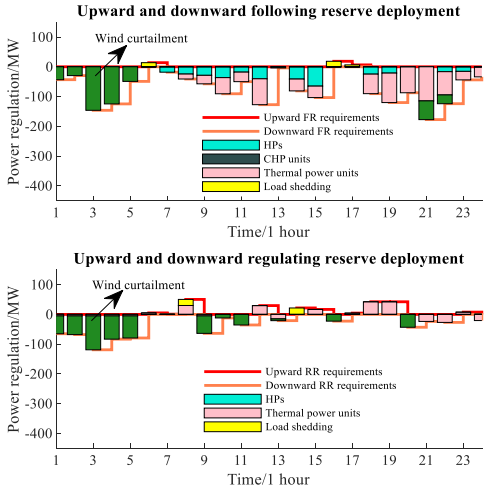

(d2) Reserve deployment of Case 1.3

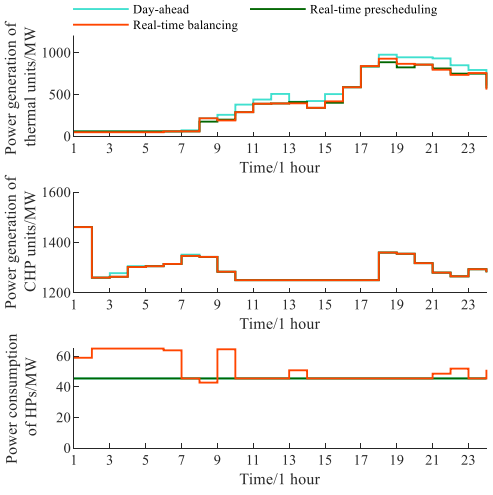

(e1) Operational plan of Case 1.4

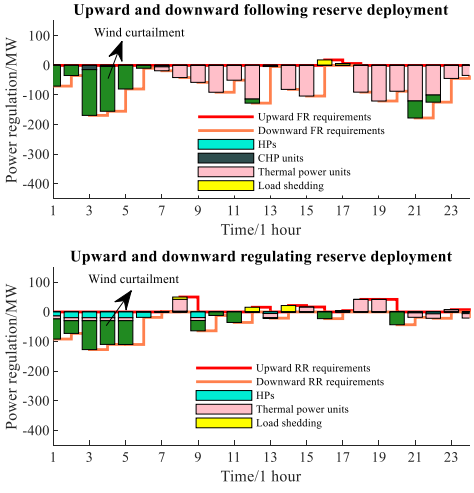

(e2) Reserve deployment of Case 1.4

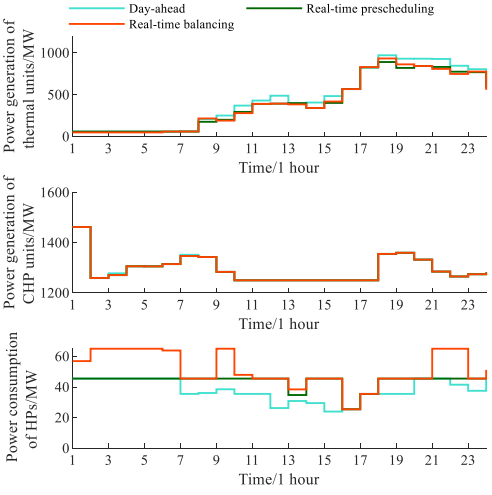

(f1) Operational plan of Case 1.5

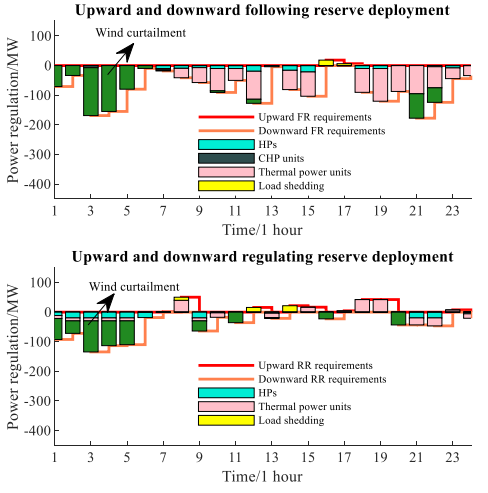

(f2) Reserve deployment of Case 1.5

Fig. 7. (*continued*).

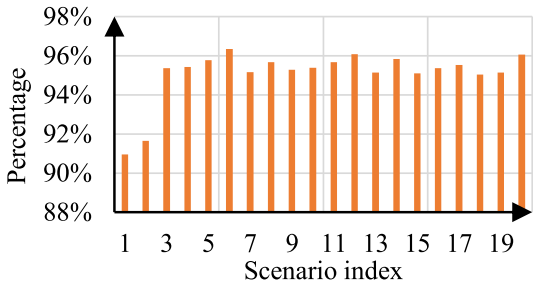

Fig. 8. Percentage of inactive transmission constraints under each scenario.

Table 3
Comparison of total calculation time between Case 2.1 and Case 2.2

Cases	Case 2.1	Case 2.2
Time of identification/s	–	2.5
Time of optimization/s	315	176
Total calculation time/s	315	178.5
Optimal obj./$	1.808864×10^6	1.808864×10^6

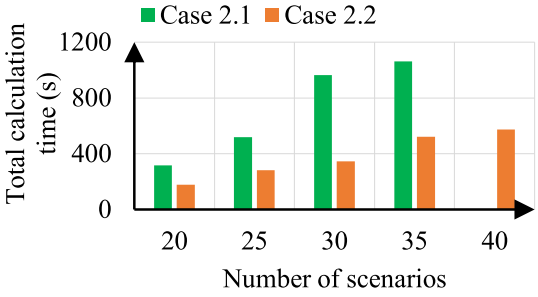

Fig. 9. Comparison of calculation time between Case 2.1 and Case 2.2 under different number of scenarios.

method in reducing computational complexity. Case 2.1 solves the original two-stage SP problem of the IEHS directly, while Case 2.2 identifies and removes the inactive transmission line constraints before the optimization. In both cases, the number of wind power output scenarios is taken as 20.

In Case 2.1, the total amount of transmission line constraints is determined by the number of transmission lines, number of time periods and number of scenarios, and is calculated as $186 \times 24 \times 20 \times 2 = 178560$, which results in a huge calculation burden for the optimization. The percentage of inactive transmission line constraints identified by the proposed analytical calculation method is given in Fig. 8. In Fig. 8, each scenario represents a possible wind power output profile. Although the wind power profile can affect the percentage of inactive transmission line constraints, there is at least 91% of transmission line constraints are inactive in each scenario, which significantly reduces the scale of the optimization problem.

Table 3 shows the comparison of total time including identification time and optimization time for two cases. In Table 3, Case 2.1 and Case 2.2 have the same optimal objective value, demonstrating that identifying and removing the inactive transmission line constraints have no influence on the decision results. Case 2.2 only takes 2.5 s to finish the identification of the inactive transmission line constraints. After removing the inactive transmission line constraints, it has less optimization time than Case 2.1 due to the decrease of computational complexity. Compared with Case 2.1, the total calculation time of Case 2.2 decreases by 43.3%.

To validate the robustness of the proposed identification method, the calculation time of Case 2.1 and Case 2.2 under different number of scenarios is tested. Fig. 9 shows the comparison results of two cases. As can be seen from Fig. 9, when the number of scenarios increases from 20 to 40, the proposed method can always be effective in saving calculation time. It should be noted that when the number of scenarios is 40, the solver cannot give the optimal solution due to the computational scale exceeds the memory. Compared with Case 2.1, Case 2.2 can reduce the total calculation time by 43.33%, 45.56%, 64.14%, and 50.85%, respectively, when the number of scenarios are 20, 25, 30, and 35. Therefore, the proposed method is robust in reducing computational complexity.

6. Conclusion

This paper proposes a day-ahead stochastic scheduling scheme for the integrated electricity and heat system, which considers the reserve provision of large-scale heat pumps and reducing the computational complexity by identifying inactive transmission line constraints. The simulation results conducted on a modified IEEE-118 bus integrated electricity and heat system validate the effectiveness of the proposed method. The main conclusions are as follows,

- Large-scale heat pumps can participate in energy scheduling and provide the following reserve and regulating reserve. By utilizing the flexibility of HPs, the total operational cost can be reduced by approximately 11%, and wind curtailment can be reduced by about 4.5%. The following reserve is more beneficial to reduce total operation cost, while the regulating reserve of large-scale heat pumps is more beneficial to reduce the real-time operational cost and wind curtailment.
- The analytical calculation method for inactive transmission line constraints considers the impact of power-to-heat devices on the power flow, which has a very fast identification speed. The total optimization time of the test system can be saved by from 43.33% to 64.14% through identifying and removing the inactive transmission line constraints.

CRediT authorship contribution statement

Menglin Zhang: Conceptualization, Methodology, Software. **Qiuwei Wu:** Conceptualization, Methodology, Software. **Jinyu Wen:** Conceptualization, Methodology. **Bo Zhou:** Conceptualization, Methodology. **Qinyue Guan:** Conceptualization, Methodology. **Jin Tan:** Conceptualization, Methodology. **Zhongwei Lin:** Conceptualization, Methodology. **Fang Fang:** Conceptualization, Methodology.

Declaration of Competing Interest

The authors declare that they have no known competing financial interests or personal relationships that could have appeared to influence the work reported in this paper.

Acknowledgement

This work was financially supported by the Innovationsfonden through the project “Using flexible district heating with heat pumps for integrated electricity and heat dispatch with renewables” (HEAT4RES), and co-financed by the MOST China through the project (2018YFE0106600).

Appendix A

Two-stage stochastic programming model of IEHS

- *Objective function*

The objective function in (A.1) and (A.2) composes the day-ahead operational cost and real-time expected cost for devices of thermal power units, CHP units, and HPs. Besides, the penalty costs for wind power curtailment and load shedding are also included in the total cost to guarantee a feasible solution.

$$minf = f_1 + \sum_{s=1}^{S} \mathrm{p}_s f_{2,s} \tag{A.1}$$

$$\begin{aligned}
f_1 &= f_1^{\mathrm{TU}} + f_1^{\mathrm{CHP}} + f_1^{\mathrm{HP}} \\
f_{2,s} &= f_{2,s}^{\mathrm{TU}} + f_{2,s}^{\mathrm{CHP}} + f_{2,s}^{\mathrm{HP}} + f_{2,s}^{\mathrm{W}} + f_{2,s}^{\mathrm{LD}} \\
f_1^{\mathrm{TU}} &= \sum_{t\in\Lambda^{\mathrm{T}}}\sum_{i\in\Psi^{\mathrm{TU}}} \left\{ \begin{array}{l} \mathrm{C}_i^{\mathrm{TU}} u_{i,t}^{\mathrm{TU}} + \mathrm{f}_i^{min,\mathrm{TU}} x_{i,t}^{\mathrm{TU}} + \sum_{k\in\Phi^{\mathrm{TU}}} \mathrm{K}_{i,k}^{\mathrm{TU}} p_{i,t,k}^{\mathrm{TU}} + \mathrm{C}_i^{\mathrm{TU,f_up,cap}} r_{i,t}^{\mathrm{TU,f_up,cap}} + \\ \mathrm{C}_i^{\mathrm{TU,f_dn,cap}} r_{i,t}^{\mathrm{TU,f_dn,cap}} + \mathrm{C}_i^{\mathrm{TU,r_up,cap}} r_{i,t}^{\mathrm{TU,r_up,cap}} + \mathrm{C}_i^{\mathrm{TU,r_dn,cap}} r_{i,t}^{\mathrm{TU,r_dn,cap}} \end{array} \right\} \\
f_1^{\mathrm{CHP}} &= \sum_{t\in\Lambda^{\mathrm{T}}}\sum_{i\in\Psi^{\mathrm{CHP}}} \left\{ \mathrm{C}_i^{\mathrm{CHP}} u_{i,t}^{\mathrm{CHP}} + f_{i,t}^{\mathrm{CHP}} + \mathrm{C}_i^{\mathrm{CHP,f_up,cap}} r_{i,t}^{\mathrm{CHP,f_up,cap}} + \mathrm{C}_i^{\mathrm{CHP,f_dn,cap}} r_{i,t}^{\mathrm{CHP,f_dn,cap}} \right\} \\
f_{i,t}^{\mathrm{CHP}} &= \sum_{j=1}^{4} \alpha_{i,t,j} \mathrm{f}_i^{\mathrm{CHP},\,j} \\
f_1^{\mathrm{HP}} &= \sum_{t\in\Lambda^{\mathrm{T}}}\sum_{i\in\Psi^{\mathrm{HP}}} \left\{ \mathrm{C}_i^{\mathrm{HP,f_up,cap}} r_{i,t}^{\mathrm{HP,f_up,cap}} + \mathrm{C}_i^{\mathrm{HP,f_dn,cap}} r_{i,t}^{\mathrm{HP,f_dn,cap}} + \mathrm{C}_i^{\mathrm{HP,r_up,cap}} r_{i,t}^{\mathrm{HP,r_up,cap}} + \mathrm{C}_i^{\mathrm{HP,r_dn,cap}} r_{i,t}^{\mathrm{HP,r_dn,cap}} \right\}
\end{aligned} \tag{A.2}$$

$$\begin{aligned}
f_{2,s}^{\mathrm{TU}} &= \sum_{t\in\Lambda^{\mathrm{T}}}\sum_{i\in\Psi^{\mathrm{TU}}} \left\{ \mathrm{C}_i^{\mathrm{TU,f_up,dep}} \Delta r_{i,t,s}^{\mathrm{TU,f_up,dep}} + \mathrm{C}_i^{\mathrm{TU,f_dn,dep}} \Delta r_{i,t,s}^{\mathrm{TU,f_dn,dep}} + \mathrm{C}_i^{\mathrm{TU,r_up,dep}} \Delta r_{i,t,s}^{\mathrm{TU,r_up,dep}} + \mathrm{C}_i^{\mathrm{TU,r_dn,dep}} \Delta r_{i,t,s}^{\mathrm{TU,r_dn,dep}} \right\} \\
f_{2,s}^{\mathrm{CHP}} &= \sum_{t\in\Lambda^{\mathrm{T}}}\sum_{i\in\Psi^{\mathrm{CHP}}} \left\{ \mathrm{C}_i^{\mathrm{CHP,f_up,dep}} \Delta r_{i,t,s}^{\mathrm{CHP,f_up,dep}} + \mathrm{C}_i^{\mathrm{CHP,f_dn,dep}} \Delta r_{i,t,s}^{\mathrm{CHP,f_dn,dep}} \right\} \\
f_{2,s}^{\mathrm{HP}} &= \sum_{t\in\Lambda^{\mathrm{T}}}\sum_{i\in\Psi^{\mathrm{HP}}} \left\{ \mathrm{C}_i^{\mathrm{HP,f_up,dep}} \Delta r_{i,t,s}^{\mathrm{HP,f_up,dep}} + \mathrm{C}_i^{\mathrm{HP,f_dn,dep}} \Delta r_{i,t,s}^{\mathrm{HP,f_dn,dep}} + \mathrm{C}_i^{\mathrm{HP,r_up,dep}} \Delta r_{i,t,s}^{\mathrm{HP,r_up,dep}} + \mathrm{C}_i^{\mathrm{HP,r_dn,dep}} \Delta r_{i,t,s}^{\mathrm{HP,r_dn,dep}} \right\} \\
f_{2,s}^{\mathrm{W}} &= \sum_{t\in\Lambda^{\mathrm{T}}}\sum_{i\in\Psi^{\mathrm{W}}} \left\{ \mathrm{C}^{\mathrm{W}} \Delta w_{i,t,s} \right\} \\
f_{2,s}^{\mathrm{LD}} &= \sum_{t\in\Lambda^{\mathrm{T}}}\sum_{i\in\Psi^{\mathrm{B}}} \left\{ \mathrm{C}^{\mathrm{LD}} \Delta L_{i,t,s} \right\}
\end{aligned}$$

- *Day-ahead scheduling constraints*

The power balance constraint is represented in (A.3).

$$\sum_{i\in\Psi^{\mathrm{TU}}} p_{i,t}^{\mathrm{TU}} + \sum_{i\in\Psi^{\mathrm{CHP}}} p_{i,t}^{\mathrm{CHP}} - \sum_{i\in\Psi^{\mathrm{HP}}} p_{i,t}^{\mathrm{HP}} + \sum_{i\in\Psi^{\mathrm{W}}} \left(\mathrm{W}_{i,t} - \Delta w_{i,t}\right) = \sum_{i\in\Psi^{\mathrm{B}}} \mathrm{L}_{i,t}, t \in \Lambda^{\mathrm{T}} \tag{A.3}$$

The operational constraints of thermal power units are represented in (A.4), where (A.4.a) is the piece-wise linearization constraint, (A.4.b) limits the maximum value for each linearized piece; (A.4.c) and (A.4.d) are upward and downward ramping constraints, respectively, with the on/off status and regulating reserve capacity included; (A.4.e) and (A.4.f) describe the available upward and downward following reserve capacities, respectively, which are limited by the ramping rate and maximum/minimum available capacity after considering regulating reserve capacity; (A.4.g)-(A.4.j) represent the on/off status constraints and minimum start-up time and shutdown time constraints of thermal power units; and (A.4.k) represents that the upward regulating reserve capacity of thermal power units should satisfy the minimum requirements to avoid the load curtailment in real-time.

$$p_{i,t}^{\mathrm{TU}} = \underline{P}_i^{\mathrm{TU}} x_{i,t}^{\mathrm{TU}} + \sum_{k\in\Phi^{\mathrm{TU}}} p_{i,t,k}^{\mathrm{TU}}, \forall t \in \Lambda^{\mathrm{T}}, \forall i \in \Psi^{\mathrm{TU}}, \forall k \in \Phi^{\mathrm{TU}} \tag{A4a}$$

$$0 \leqslant p_{i,t,k}^{\mathrm{TU}} \leqslant \overline{P}_{i,k}^{\mathrm{TU}}, \forall t \in \Lambda^{\mathrm{T}}, \forall i \in \Psi^{\mathrm{TU}}, \forall k \in \Phi^{\mathrm{TU}} \tag{A4b}$$

$$p_{i,t}^{\mathrm{TU}} - p_{i,t-1}^{\mathrm{TU}} \leqslant \mathrm{U}_i^{\mathrm{TU}} \left(1 - u_{i,t}^{\mathrm{TU}}\right) + \left(\overline{P}_i^{\mathrm{TU}} - r_{i,t}^{\mathrm{TU,r\_up,cap}}\right) u_{i,t}^{\mathrm{TU}}, \ \forall t \in \Lambda^{\mathrm{T}}, \forall i \in \Psi^{\mathrm{TU}} \tag{A4c}$$

$$p_{i,t-1}^{\mathrm{TU}} - p_{i,t}^{\mathrm{TU}} \leqslant \mathrm{D}_i^{\mathrm{TU}} (1 - v_{i,t}^{\mathrm{TU}}) + \left(\overline{P}_i^{\mathrm{TU}} - r_{i,t}^{\mathrm{TU,r\_up,cap}}\right) v_{i,t}^{\mathrm{TU}}, \ \forall t \in \Lambda^{\mathrm{T}}, \forall i \in \Psi^{\mathrm{TU}} \tag{A4d}$$

$$r_{i,t}^{\mathrm{TU,f\_up,cap}} \leqslant min\{\mathrm{U}_i^{\mathrm{TU}} x_{i,t}^{\mathrm{TU}}, \left(\overline{P}_i^{\mathrm{TU}} - r_{i,t}^{\mathrm{TU,r\_up,cap}}\right) x_{i,t}^{\mathrm{TU}} - p_{i,t}^{\mathrm{TU}}\}, \quad \forall t \in \Lambda^{\mathrm{T}}, \forall i \in \Psi^{\mathrm{TU}} \tag{A4e}$$

$$r_{i,t}^{\mathrm{TU,f\_dn,cap}} \leqslant min\left\{\mathrm{D}_i^{\mathrm{TU}} x_{i,t}^{\mathrm{TU}}, p_{i,t}^{\mathrm{TU}} - \left(\underline{P}_i^{\mathrm{TU}} + r_{i,t}^{\mathrm{TU,r\_dn,cap}}\right) x_{i,t}^{\mathrm{TU}}\right\}, \quad \forall t \in \Lambda^{\mathrm{T}}, \forall i \in \Psi^{\mathrm{TU}} \tag{A4f}$$

$$u_{i,t}^{\mathrm{TU}} - v_{i,t}^{\mathrm{TU}} = x_{i,t}^{\mathrm{TU}} - x_{i,t-1}^{\mathrm{TU}}, \forall t \in \Lambda^{\mathrm{T}}, \forall i \in \Psi^{\mathrm{TU}} \tag{A4g}$$

$$u_{i,t}^{\mathrm{TU}} + v_{i,t}^{\mathrm{TU}} \leqslant 1, \forall t \in \Lambda^{\mathrm{T}}, \forall i \in \Psi^{\mathrm{TU}} \tag{A4h}$$

$$x_{i,t}^{\mathrm{TU}} - x_{i,t-1}^{\mathrm{TU}} \leqslant x_{i,\tau}^{\mathrm{TU}} \ , \ \forall \tau \in [t+1, min\{\mathrm{N}_T, t + \mathrm{t}_{\mathrm{st},i}^{\mathrm{TU}} - 1\}] \tag{A4i}$$

$$x_{i,t-1}^{\mathrm{TU}} - x_{i,t}^{\mathrm{TU}} \leqslant 1 - x_{i,\tau}^{\mathrm{TU}}, \quad \forall \tau \in [t+1, min\{\mathrm{N}_{\mathrm{T}}, t + \mathrm{t}_{\mathrm{dn},i}^{\mathrm{TU}} - 1\}] \tag{A4j}$$

$$\sum_{i \in \Psi^{\mathrm{TU}}} r_{i,t}^{\mathrm{TU,r\_up,cap}} \geqslant \mathrm{R}_t^{\mathrm{r\_up,total}}, \quad \forall t \in \Lambda^{\mathrm{T}} \tag{A4k}$$

The operational constraints of CHP units are represented in (A.5) [36], where (A.5.a) and (A.5.b) represent the power and heat production of condensing CHP unit *i*, respectively, which are coupled by four vertex coefficients of the operational region; (A.5.c) represents the summation of four vertex coefficients is determined by the on/off status of CHP unit *i*; (A.5.d) limits the four vertex coefficients within the range [0, 1]; (A.5.e) and (A.5.f) represent the upward and downward ramping constraints of CHP units, respectively, with the on/off status included; (A.5.g) and (A.5.h) are the upward and downward following reserve capacity of CHP unit *i*, respectively; and (A.5.i)-(A.5.l) represent the on/off status constraints and minimum start-up time and shutdown time constraints of CHP units.

$$p_{i,t}^{\mathrm{CHP}} = \sum_{j=1}^{4} \alpha_{i,t,j} \mathrm{p}_i^{\mathrm{CHP},j}, \forall t \in \Lambda^{\mathrm{T}}, \forall i \in \Psi^{\mathrm{CHP}} \tag{A.5.a}$$

$$h_{i,t}^{\mathrm{CHP}} = \sum_{j=1}^{4} \alpha_{i,t,j} \mathrm{h}_i^{\mathrm{CHP},j}, \forall t \in \Lambda^{\mathrm{T}}, \forall i \in \Psi^{\mathrm{CHP}} \tag{A.5.b}$$

$$\sum_{j=1}^{4} \alpha_{i,t,j} = x_{i,t}^{\mathrm{CHP}}, \forall t \in \Lambda^{\mathrm{T}}, \forall i \in \Psi^{\mathrm{CHP}} \tag{A.5.c}$$

$$0 \leqslant \alpha_{i,t,j} \leqslant 1, \forall t \in \Lambda^{\mathrm{T}}, \forall i \in \Psi^{\mathrm{CHP}} \tag{A.5.d}$$

$$p_{i,t}^{\mathrm{CHP}} - p_{i,t-1}^{\mathrm{CHP}} \leqslant \mathrm{U}_i^{\mathrm{CHP}}(1 - u_{i,t}^{\mathrm{CHP}}) + \overline{P}_i^{\mathrm{CHP}} u_{i,t}^{\mathrm{CHP}} \ , \ \forall t \in \Lambda^{\mathrm{T}}, \forall i \in \Psi^{\mathrm{CHP}} \tag{A.5.e}$$

$$p_{i,t-1}^{\mathrm{CHP}} - p_{i,t}^{\mathrm{CHP}} \leqslant \mathrm{D}_i^{\mathrm{CHP}}(1 - v_{i,t}^{\mathrm{CHP}}) + \overline{P}_i^{\mathrm{CHP}} v_{i,t}^{\mathrm{CHP}}, \ \forall t \in \Lambda^{\mathrm{T}}, \forall i \in \Psi^{\mathrm{CHP}} \tag{A.5.f}$$

$$r_{i,t}^{\mathrm{CHP,f\_up,cap}} \leqslant min\left\{ \mathrm{U}_i^{\mathrm{CHP}} x_{i,t}^{\mathrm{CHP}}, \overline{P}_i^{\mathrm{CHP}} x_{i,t}^{\mathrm{CHP}} - p_{i,t}^{\mathrm{CHP}} \right\}, \quad \forall t \in \Lambda^{\mathrm{T}}, \forall i \in \Psi^{\mathrm{CHP}} \tag{A.5.g}$$

$$r_{i,t}^{\mathrm{CHP,f\_dn,cap}} \leqslant min\left\{ \mathrm{D}_i^{\mathrm{CHP}} x_{i,t}^{\mathrm{CHP}}, p_{i,t}^{\mathrm{CHP}} - \underline{P}_i^{\mathrm{CHP}} x_{i,t}^{\mathrm{CHP}} \right\}, \quad \forall t \in \Lambda^{\mathrm{T}}, \forall i \in \Psi^{\mathrm{CHP}} \tag{A.5.h}$$

$$u_{i,t}^{\mathrm{CHP}} - v_{i,t}^{\mathrm{CHP}} = x_{i,t}^{\mathrm{CHP}} - x_{i,t-1}^{\mathrm{CHP}}, \forall t \in \Lambda^{\mathrm{T}}, \forall i \in \Psi^{\mathrm{CHP}} \tag{A.5.i}$$

$$u_{i,t}^{\mathrm{CHP}} + v_{i,t}^{\mathrm{CHP}} \leqslant 1, \forall t \in \Lambda^{\mathrm{T}}, \forall i \in \Psi^{\mathrm{CHP}} \tag{A.5.j}$$

$$x_{i,t}^{\mathrm{CHP}} - x_{i,t-1}^{\mathrm{CHP}} \leqslant x_{i,\tau}^{\mathrm{CHP}} \ , \ \forall \tau \in [t+1, min\{\mathrm{N}_T, t + \mathrm{t}_{\mathrm{st},i}^{\mathrm{CHP}} - 1\}] \tag{A.5.k}$$

$$x_{i,t-1}^{\mathrm{CHP}} - x_{i,t}^{\mathrm{CHP}} \leqslant 1 - x_{i,\tau}^{\mathrm{CHP}}, \quad \forall \tau \in [t+1, min\{\mathrm{N}_{\mathrm{T}}, t + \mathrm{t}_{\mathrm{dn},i}^{\mathrm{CHP}} - 1\}] \tag{A.5.l}$$

The operational constraints of large-scale HPs are represented in (A.6), where (A.6.a) represents the power consumption constraint of HPs with the on/off status, which considers the coupling with upward and downward regulating reserve capacities; (A.6.b) and (A.6.c) limit the available downward and upward following reserve capacities, respectively; and (A.6.d) represents the coupling relationship between power consumption and heat production.

$$\left(\underline{P}_i^{\mathrm{HP}} + r_{i,t}^{\mathrm{HP,r\_up,cap}}\right) x_{i,t}^{\mathrm{HP}} \leqslant p_{i,t}^{\mathrm{HP}} \leqslant \left(\overline{P}_i^{\mathrm{HP}} - r_{i,t}^{\mathrm{HP,r\_dn,cap}}\right) x_{i,t}^{\mathrm{HP}}, \quad \forall t \in \Lambda^{\mathrm{T}}, \forall i \in \Psi^{\mathrm{HP}} \tag{A.6.a}$$

$$r_{i,t}^{\mathrm{HP,f\_dn,cap}} \leqslant \left(\overline{P}_i^{\mathrm{HP}} - r_{i,t}^{\mathrm{HP,r\_dn,cap}}\right) x_{i,t}^{\mathrm{HP}} - p_{i,t}^{\mathrm{HP}}, \quad \forall t \in \Lambda^{\mathrm{T}}, \forall i \in \Psi^{\mathrm{HP}} \tag{A.6.b}$$

$$r_{i,t}^{\mathrm{HP,f\_up,cap}} \leqslant p_{i,t}^{\mathrm{HP}} - \left(\underline{P}_i^{\mathrm{HP}} + r_{i,t}^{\mathrm{HP,r\_up,cap}}\right) x_{i,t}^{\mathrm{HP}}, \quad \forall t \in \Lambda^{\mathrm{T}}, \forall i \in \Psi^{\mathrm{HP}} \tag{A.6.c}$$

$$h_{i,t}^{\mathrm{HP}} = \eta_i^{\mathrm{HP}} p_{i,t}^{\mathrm{HP}}, \forall t \in \Lambda^{\mathrm{T}}, \forall i \in \Psi^{\mathrm{HP}} \tag{A.6.d}$$

The transmission line constraints based on the direct current power flow method is represented in (A.7).

$$\left| \sum_{i \in \Theta^{\mathrm{TU},d}} \mathrm{g}_{d,l}^{\mathrm{TU}} p_{i,t}^{\mathrm{TU}} + \sum_{i \in \Theta^{\mathrm{CHP},d}} \mathrm{g}_{d,l}^{\mathrm{CHP}} p_{i,t}^{\mathrm{CHP}} + \sum_{i \in \Theta^{\mathrm{W},d}} \mathrm{g}_{d,l}^{\mathrm{W}} \left(\mathrm{W}_{i,t} - \Delta w_{i,t}\right) - \sum_{i \in \Theta^{\mathrm{HP},d}} \mathrm{g}_{d,l}^{\mathrm{HP}} p_{i,t}^{\mathrm{HP}} - \sum_{i \in \Psi^{\mathrm{B}}} \mathrm{g}_{d,l}^{\mathrm{B}} \mathrm{L}_{i,t} \right| \leqslant \mathrm{f}_l^{max}, \forall t \in \Lambda^{\mathrm{T}}, \forall d \in \Psi^{\mathrm{B}}, \forall l \in \Psi^{\mathrm{L}} \tag{A.7}$$

The heat balance constraint is represented in (A.8).

$$\sum_{i\in\Omega^{\mathrm{CHP},d}} h_{i,t}^{\mathrm{CHP}} + \sum_{i\in\Omega^{\mathrm{HP},d}} h_{i,t}^{\mathrm{HP}} - \sum_{i\in\Omega^{\mathrm{ST},d}} h_{i,t}^{\mathrm{ST}} = \mathrm{L}_d^{\mathrm{heat}}, \quad \forall t\in\Lambda^{\mathrm{T}},\ \forall d\in\Phi^{\mathrm{Heat}} \tag{A.8}$$

The operational constraints of STs are represented in (A.9), where (A.9.a) limits the maximum charging/discharging rate of STs; (A.9.b) reflects the changes of heat energy level in STs; and (A.9.c) limits the maximum and minimum heat energy levels in STs.

$$-\overline{h}_i^{\mathrm{ST}} \leqslant h_{i,t}^{\mathrm{ST}} \leqslant \overline{h}_i^{\mathrm{ST}}, \forall t\in\Lambda^{\mathrm{T}}, \forall i\in\Psi^{\mathrm{ST}} \tag{A.9.a}$$

$$H_{i,t+1}^{\mathrm{ST}} = H_{i,t}^{\mathrm{ST}} + h_{i,t}^{\mathrm{ST}}, \forall t\in\Lambda^{\mathrm{T}}, \forall i\in\Psi^{\mathrm{ST}} \tag{A.9.b}$$

$$\underline{H}_i^{\mathrm{ST}} \leqslant H_{i,t}^{\mathrm{ST}} \leqslant \overline{H}_i^{\mathrm{ST}}, \forall t\in\Lambda^{\mathrm{T}}, \forall i\in\Psi^{\mathrm{ST}} \tag{A.9.c}$$

- *Real-time operational constraints*

Including real-time operational constraints in day-ahead scheduling is to make the day-ahead schedule can adapt to possible realizations of wind power in real-time.

Each possible realization (represented by a scenario) of real-time wind power outputs $\left[W_{i,1,s}, W_{i,2,s}, \cdots, W_{i,t,s}, \cdots, W_{i,T,s}\right]$, $(i=1,2,\cdots,N_J, \forall s)$ corresponds to a set of real-time operational constraints. Since each real-time scenario of wind power outputs have a deviation with day-ahead forecast values, the power rebalance will be necessary for each real-time scenario, which can be achieved by reserve deployment from thermal power units, CHP units, and large-scale HPs. At the same time, since the reserve deployment and heat production are coupled for CHP units and large-scale HPs, the reserve deployment of these two devices may cause the heat imbalance. Therefore, the heat regulation of STs will also be conducted to ensure the heat balance.

The power rebalance constraint for each scenario is represented in (A.10), which is achieved by deploying the following reserve and regulating reserve, and conducting wind power curtailment and load shedding, simultaneously.

$$\begin{aligned}\sum_{i\in\Psi^{\mathrm{TU}}}\left(\Delta r_{i,t,s}^{\mathrm{TU,f\_up,dep}} - \Delta r_{i,t,s}^{\mathrm{TU,f\_dn,dep}} + \Delta r_{i,t,s}^{\mathrm{TU,r\_up,dep}} - \Delta r_{i,t,s}^{\mathrm{TU,r\_dn,dep}}\right) - \sum_{i\in\Psi^{\mathrm{HP}}}\left(\Delta r_{i,t,s}^{\mathrm{HP,f\_dn,dep}} - \Delta r_{i,t,s}^{\mathrm{TU,f\_up,dep}} + \Delta r_{i,t,s}^{\mathrm{TU,r\_dn,dep}} - \Delta r_{i,t,s}^{\mathrm{TU,r\_up,dep}}\right) + \\ \sum_{i\in\Psi^{\mathrm{CHP}}}\left(\Delta r_{i,t,s}^{\mathrm{CHP,f\_up,dep}} - \Delta r_{i,t,s}^{\mathrm{CHP,f\_dn,dep}}\right) + \sum_{i\in\Psi^{\mathrm{W}}}\left(\mathrm{W}_{i,t,s} - \mathrm{W}_{i,t} - \Delta w_{i,t,s} + \Delta w_{i,t}\right) = \sum_{i\in\Psi^{\mathrm{B}}} - \Delta L_{i,t,s}, \forall t\in\Lambda^{\mathrm{T}}, \forall s\in\Psi^{\mathrm{S}}\end{aligned} \tag{A.10}$$

The real-time constraints of CHP units for each scenario are represented in (A.11), where (A.11.a) and (A.11.b) ensure the upward and downward following reserve deployments in each scenario no more than the day-ahead following reserve capacity; (A.11.c)-(A.11.f) utilize the linear combination of vertex regulation coefficients to represent the upward and downward following reserve deployment and coupled heat regulation in each scenario; (A.11.g)-(A.11.h) represent the relationship of the vertex regulation coefficient of four vertices [36]; (A.11.i)-(A.11.k) limit the range of vertex regulation coefficients; and (A.11.l)-(A.11.m) describe the upward/downward ramping constraints after reserve deployment.

$$0 \leqslant \Delta r_{i,t,s}^{\mathrm{CHP,f\_up,dep}} \leqslant r_{i,t}^{\mathrm{CHP,f\_up,cap}}, \quad \forall t\in\Lambda^{\mathrm{T}}, \forall i\in\Psi^{\mathrm{CHP}}, \forall s\in\Psi^{\mathrm{S}} \tag{A.11.a}$$

$$0 \leqslant \Delta r_{i,t,s}^{\mathrm{CHP,f\_dn,dep}} \leqslant r_{i,t}^{\mathrm{CHP,f\_dn,cap}}, \quad \forall t\in\Lambda^{\mathrm{T}}, \forall i\in\Psi^{\mathrm{CHP}}, \forall s\in\Psi^{\mathrm{S}} \tag{A.11.b}$$

$$\Delta r_{i,t,s}^{\mathrm{CHP,f\_up,dep}} = \sum_{j=1}^{4} \Delta\alpha_{i,t,s,j}^{\mathrm{f\_up}} \mathrm{p}_i^{\mathrm{CHP},\,j}, \quad \forall t\in\Lambda^{\mathrm{T}}, \forall i\in\Psi^{\mathrm{CHP}}, \forall s\in\Psi^{\mathrm{S}} \tag{A.11.c}$$

$$\Delta r_{i,t,s}^{\mathrm{CHP,f\_dn,dep}} = \sum_{j=1}^{4} \Delta\alpha_{i,t,s,j}^{\mathrm{f\_dn}} \mathrm{p}_i^{\mathrm{CHP},\,j}, \quad \forall t\in\Lambda^{\mathrm{T}}, \forall i\in\Psi^{\mathrm{CHP}}, \forall s\in\Psi^{\mathrm{S}} \tag{A.11.d}$$

$$\Delta h_{i,t,s}^{\mathrm{CHP,f\_up,dep}} = \sum_{j=1}^{4} \Delta\alpha_{i,t,s,j}^{\mathrm{f\_up}} \mathrm{h}_{i,t}^{\mathrm{CHP},\,j}, \forall t\in\Lambda^{\mathrm{T}}, \forall i\in\Psi^{\mathrm{CHP}}, \forall s\in\Psi^{\mathrm{S}} \tag{A.11.e}$$

$$\Delta h_{i,t,s}^{\mathrm{CHP,f\_dn,dep}} = \sum_{j=1}^{4} \Delta\alpha_{i,t,s,j}^{\mathrm{f\_dn}} \mathrm{h}_{i,t}^{\mathrm{CHP},\,j}, \forall t\in\Lambda^{\mathrm{T}}, \forall i\in\Psi^{\mathrm{CHP}}, \forall s\in\Psi^{\mathrm{S}} \tag{A.11.f}$$

$$\sum_{j=1}^{4} \Delta\alpha_{i,t,s,j}^{\mathrm{f\_up}} = 0, \forall t\in\Lambda^{\mathrm{T}}, \forall i\in\Psi^{\mathrm{CHP}}, \forall s\in\Psi^{\mathrm{S}} \tag{A.11.g}$$

$$\sum_{j=1}^{4} \Delta\alpha_{i,t,s,j}^{\mathrm{f\_dn}} = 0, \forall t\in\Lambda^{\mathrm{T}}, \forall i\in\Psi^{\mathrm{CHP}}, \forall s\in\Psi^{\mathrm{S}} \tag{A.11.h}$$

$$0 \leqslant \alpha_{i,t,j} + \Delta\alpha_{i,t,s,j}^{\mathrm{f\_up}} \leqslant 1, \forall j, \forall t\in\Lambda^{\mathrm{T}}, \forall i\in\Psi^{\mathrm{CHP}}, \forall s\in\Psi^{\mathrm{S}} \tag{A.11.i}$$

$$0 \leqslant \alpha_{i,t,j} - \Delta\alpha_{i,t,s,j}^{\mathrm{f\_dn}} \leqslant 1, \forall j, \forall t\in\Lambda^{\mathrm{T}}, \forall i\in\Psi^{\mathrm{CHP}}, \forall s\in\Psi^{\mathrm{S}} \tag{A.11.j}$$

$$0 \leqslant \alpha_{i,t,j} + \Delta\alpha_{i,t,s,j}^{\mathrm{f\_up}} - \Delta\alpha_{i,t,s,j}^{\mathrm{f\_dn}} \leqslant 1, \forall j, \forall t\in\Lambda^{\mathrm{T}}, \forall i\in\Psi^{\mathrm{CHP}}, \forall s\in\Psi^{\mathrm{S}} \tag{A.11.k}$$

$$\left(p_{i,t}^{\mathrm{CHP}} + \Delta r_{i,t,s}^{\mathrm{CHP,f\_up,dep}} - \Delta r_{i,t,s}^{\mathrm{CHP,f\_dn,dep}}\right) - \left(p_{i,t-1}^{\mathrm{CHP}} + \Delta r_{i,t-1,s}^{\mathrm{CHP,f\_up,dep}} - \Delta r_{i,t-1,s}^{\mathrm{CHP,f\_dn,dep}}\right) \leqslant \mathrm{U}_i^{\mathrm{CHP}}\left(1 - u_{i,t}^{\mathrm{CHP}}\right) + \overline{P}_i^{\mathrm{CHP}} u_{i,t}^{\mathrm{CHP}} \tag{A.11.l}$$

$$\left(p_{i,t-1}^{\mathrm{CHP}} + \Delta r_{i,t-1,s}^{\mathrm{CHP,f\_up,dep}} - \Delta r_{i,t-1,s}^{\mathrm{CHP,f\_dn,dep}}\right) - \left(p_{i,t}^{\mathrm{CHP}} + \Delta r_{i,t,s}^{\mathrm{CHP,f\_up,dep}} - \Delta r_{i,t,s}^{\mathrm{CHP,f\_dn,dep}}\right) \leqslant \mathrm{D}_i^{\mathrm{CHP}}\left(1 - v_{i,t}^{\mathrm{CHP}}\right) + \overline{P}_i^{\mathrm{CHP}} v_{i,t}^{\mathrm{CHP}} \tag{A.11.m}$$

The real-time constraints of thermal power units for each scenario are represented in (A.12), where (A.12.a) and (A.12.b) ensure the upward and downward following reserve deployments in each scenario no more than the day-ahead following reserve capacity, respectively; (A.12.c) and (A.12.d) ensure the upward and downward regulating reserve deployments in each scenario no more than the day-ahead regulating reserve capacity, respectively; and (A.12.e) and (A.12.f) describe the upward/downward ramping constraints after reserve deployment.

$$0 \leqslant \Delta r_{i,t,s}^{\mathrm{TU,f\_up,dep}} \leqslant r_{i,t}^{\mathrm{TU,f\_up,cap}}, \quad \forall t \in \Lambda^{\mathrm{T}}, \forall i \in \Psi^{\mathrm{TU}}, \forall s \in \Psi^{\mathrm{S}} \tag{A.12.a}$$

$$0 \leqslant \Delta r_{i,t,s}^{\mathrm{TU,f\_dn,dep}} \leqslant r_{i,t}^{\mathrm{TU,f\_dn,cap}}, \quad \forall t \in \Lambda^{\mathrm{T}}, \forall i \in \Psi^{\mathrm{TU}}, \forall s \in \Psi^{\mathrm{S}} \tag{A.12.b}$$

$$0 \leqslant \Delta r_{i,t,s}^{\mathrm{TU,r\_up,dep}} \leqslant r_{i,t}^{\mathrm{TU,r\_up,cap}}, \quad \forall t \in \Lambda^{\mathrm{T}}, \forall i \in \Psi^{\mathrm{TU}}, \forall s \in \Psi^{\mathrm{S}} \tag{A.12.c}$$

$$0 \leqslant \Delta r_{i,t,s}^{\mathrm{TU,r\_dn,dep}} \leqslant r_{i,t}^{\mathrm{TU,r\_dn,cap}}, \quad \forall t \in \Lambda^{\mathrm{T}}, \forall i \in \Psi^{\mathrm{TU}}, \forall s \in \Psi^{\mathrm{S}} \tag{A.12.d}$$

$$\begin{aligned}\left(p_{i,t}^{\mathrm{TU}} + \Delta r_{i,t,s}^{\mathrm{TU,f\_up,dep}} - \Delta r_{i,t,s}^{\mathrm{TU,f\_dn,dep}} + \Delta r_{i,t,s}^{\mathrm{TU,r\_up,dep}} - \Delta r_{i,t,s}^{\mathrm{TU,r\_dn,dep}}\right) - \left(p_{i,t-1}^{\mathrm{TU}} + \Delta r_{i,t-1,s}^{\mathrm{TU,f\_up,dep}} - \Delta r_{i,t-1,s}^{\mathrm{TU,f\_dn,dep}} + \Delta r_{i,t-1,s}^{\mathrm{TU,r\_up,dep}} - \Delta r_{i,t-1,s}^{\mathrm{TU,r\_dn,dep}}\right) \\ \leqslant \mathrm{U}_i^{\mathrm{TU}}\left(1 - u_{i,t}^{\mathrm{TU}}\right) + \overline{P}_i^{\mathrm{TU}} u_{i,t}^{\mathrm{TU}}\end{aligned} \tag{A.12.e}$$

$$\begin{aligned}\left(p_{i,t-1}^{\mathrm{TU}} + \Delta r_{i,t-1,s}^{\mathrm{TU,f\_up,dep}} - \Delta r_{i,t-1,s}^{\mathrm{TU,f\_dn,dep}} + \Delta r_{i,t-1,s}^{\mathrm{TU,r\_up,dep}} - \Delta r_{i,t-1,s}^{\mathrm{TU,r\_dn,dep}}\right) - \left(p_{i,t}^{\mathrm{TU}} + \Delta r_{i,t,s}^{\mathrm{TU,f\_up,dep}} - \Delta r_{i,t,s}^{\mathrm{TU,f\_dn,dep}} + \Delta r_{i,t,s}^{\mathrm{TU,r\_up,dep}} - \Delta r_{i,t,s}^{\mathrm{TU,r\_dn,dep}}\right) \\ \leqslant \mathrm{D}_i^{\mathrm{TU}}\left(1 - v_{i,t}^{\mathrm{TU}}\right) + \overline{P}_i^{\mathrm{TU}} v_{i,t}^{\mathrm{TU}}\end{aligned} \tag{A.12.f}$$

The real-time constraints of large-scale HPs for each scenario are represented in (A.13), where (A.13.a)-(A.13.d) ensure the following reserve and regulating reserve deployment of large-scale HPs are no more than day-ahead following and regulating reserve capacities; and (A.13.e)-(A.13.h) represent that the heat regulation of large-scale HPs are related to their upward/downward following and regulating reserve deployment.

$$0 \leqslant \Delta r_{i,t,s}^{\mathrm{HP,f\_up,dep}} \leqslant r_{i,t}^{\mathrm{HP,f\_up,cap}}, \quad \forall t \in \Lambda^{\mathrm{T}}, \forall i \in \Psi^{\mathrm{HP}}, \forall s \in \Psi^{\mathrm{S}} \tag{A.13.a}$$

$$0 \leqslant \Delta r_{i,t,s}^{\mathrm{HP,f\_dn,dep}} \leqslant r_{i,t}^{\mathrm{HP,f\_dn,cap}}, \quad \forall t \in \Lambda^{\mathrm{T}}, \forall i \in \Psi^{\mathrm{HP}}, \forall s \in \Psi^{\mathrm{S}} \tag{A.13.b}$$

$$0 \leqslant \Delta r_{i,t,s}^{\mathrm{HP,r\_up,dep}} \leqslant r_{i,t}^{\mathrm{HP,r\_dn,cap}}, \quad \forall t \in \Lambda^{\mathrm{T}}, \forall i \in \Psi^{\mathrm{HP}}, \forall s \in \Psi^{\mathrm{S}} \tag{A.13.c}$$

$$0 \leqslant \Delta r_{i,t,s}^{\mathrm{HP,r\_dn,dep}} \leqslant r_{i,t}^{\mathrm{HP,r\_dn,cap}}, \quad \forall t \in \Lambda^{\mathrm{T}}, \forall i \in \Psi^{\mathrm{HP}}, \forall s \in \Psi^{\mathrm{S}} \tag{A.13.d}$$

$$\Delta h_{i,t,s}^{\mathrm{HP,f\_dn}} = \eta_i^{\mathrm{HP}} \Delta r_{i,t,s}^{\mathrm{HP,f\_dn,dep}}, \forall t \in \Lambda^{\mathrm{T}}, \forall i \in \Psi^{\mathrm{HP}} \tag{A.13.e}$$

$$\Delta h_{i,t,s}^{\mathrm{HP,f\_up}} = \eta_i^{\mathrm{HP}} \Delta r_{i,t,s}^{\mathrm{HP,f\_up,dep}}, \forall t \in \Lambda^{\mathrm{T}}, \forall i \in \Psi^{\mathrm{HP}} \tag{A.13.f}$$

$$\Delta h_{i,t,s}^{\mathrm{HP,r\_dn}} = \eta_i^{\mathrm{HP}} \Delta r_{i,t,s}^{\mathrm{HP,r\_dn,dep}}, \forall t \in \Lambda^{\mathrm{T}}, \forall i \in \Psi^{\mathrm{HP}} \tag{A.13.g}$$

$$\Delta h_{i,t,s}^{\mathrm{HP,r\_up}} = \eta_i^{\mathrm{HP}} \Delta r_{i,t,s}^{\mathrm{HP,r\_up,dep}}, \forall t \in \Lambda^{\mathrm{T}}, \forall i \in \Psi^{\mathrm{HP}} \tag{A.13.h}$$

The wind power curtailment and load shedding constraints under each scenario are described in (A.14) and (A.15), respectively.

$$0 \leqslant \Delta w_{i,t,s} \leqslant \mathrm{W}_{i,t,s}, \quad \forall t \in \Lambda^{\mathrm{T}}, \forall i \in \Psi^{\mathrm{W}} \tag{A.14}$$

$$0 \leqslant \Delta L_{i,t,s} \leqslant \mathrm{L}_{i,t}, \quad \forall t \in \Lambda^{\mathrm{T}}, \forall i \in \Psi^{\mathrm{B}} \tag{A.15}$$

The transmission line constraints for each scenario after reserve deployment is described in (A.16).

$$\left|\begin{aligned}&\sum_{i\in\Theta^{\mathrm{TU,d}}} \mathrm{g}_{d,l}^{\mathrm{TU}}\left(p_{i,t}^{\mathrm{TU}} + \Delta r_{i,t,s}^{\mathrm{TU,f\_up,dep}} - \Delta r_{i,t,s}^{\mathrm{TU,f\_dn,dep}} + \Delta r_{i,t,s}^{\mathrm{TU,r\_up,dep}} - \Delta r_{i,t,s}^{\mathrm{TU,r\_dn,dep}}\right) + \sum_{i\in\Theta^{\mathrm{CHP,d}}} \mathrm{g}_{d,l}^{\mathrm{CHP}}\left(p_{i,t}^{\mathrm{CHP}} + \Delta r_{i,t,s}^{\mathrm{CHP,f\_up,dep}} - \Delta r_{i,t,s}^{\mathrm{CHP,f\_dn,dep}}\right) + \\ &\sum_{i\in\Theta^{\mathrm{W,d}}} \mathrm{g}_{d,l}^{\mathrm{W}}\left(\mathrm{W}_{i,t,s} - \Delta w_{i,t,s}\right) - \sum_{i\in\Theta^{\mathrm{HP,d}}} \mathrm{g}_{d,l}^{\mathrm{HP}}\left(p_{i,t}^{\mathrm{HP}} + \Delta r_{i,t,s}^{\mathrm{HP,f\_dn,dep}} - \Delta r_{i,t,s}^{\mathrm{HP,f\_up,dep}} + \Delta r_{i,t,s}^{\mathrm{HP,r\_dn,dep}} - \Delta r_{i,t,s}^{\mathrm{HP,r\_up,dep}}\right) - \sum_{i\in\Psi^{\mathrm{B}}} \mathrm{g}_{d,l}^{\mathrm{B}}\left(\mathrm{L}_{i,t} - \Delta L_{i,t,s}\right)\end{aligned}\right| \leqslant \mathrm{f}_l^{max} \tag{A.16}$$

Heat rebalance constraints under each scenario

$$\begin{aligned}\sum_{i\in\Omega^{\mathrm{CHP},d}} \left(h_{i,t}^{\mathrm{CHP}} + \Delta h_{i,t,s}^{\mathrm{CHP,f\_up}} - \Delta h_{i,t,s}^{\mathrm{CHP,f\_dn}}\right) + \sum_{i\in\Omega^{\mathrm{HP},d}} \left(h_{i,t}^{\mathrm{HP}} + \Delta h_{i,t,s}^{\mathrm{HP,f\_dn}} - \Delta h_{i,t,s}^{\mathrm{HP,f\_up}} + \Delta h_{i,t,s}^{\mathrm{HP,r\_dn}} - \Delta h_{i,t,s}^{\mathrm{HP,r\_up}}\right) - \sum_{i\in\Omega^{\mathrm{ST},d}} h_{i,t,s}^{\mathrm{ST}} = \mathrm{L}_d^{\mathrm{heat}}, \\ \forall t \in \Lambda^{\mathrm{T}}, \forall s \in \Psi^{\mathrm{S}}, \forall d \in \Phi^{\mathrm{Heat}}\end{aligned} \tag{A.17}$$

The heat regulation constraints of STs for each scenario are represented in (A.18), which are similar to (A.9), representing the charging/discharging rate, changes of heat energy level, and limits for heat energy level in STs.

$$-\overline{h}_i^{\mathrm{ST}} \leqslant h_{i,t,s}^{\mathrm{ST}} \leqslant \overline{h}_i^{\mathrm{ST}}, \forall t \in \Lambda^{\mathrm{T}}, \forall i \in \Psi^{\mathrm{ST}} \tag{A.18.a}$$

$$H^{ST}_{i,t+1,s} = H^{ST}_{i,t,s} + h^{ST}_{i,t,s}, \forall t \in \Lambda^{T}, \forall i \in \Psi^{ST} \quad \text{(A.18.b)}$$

$$\underline{H}^{ST}_{i} \leqslant H^{ST}_{i,t,s} \leqslant \overline{H}^{ST}_{i}, \forall t \in \Lambda^{T}, \forall i \in \Psi^{ST} \quad \text{(A.18.c)}$$

References

[1] Paris Agreement. Report of the Conference of the Parties to the United Nations Framework Convention on Climate Change; 2015.
[2] Yang X, Xu C, Zhang Y, Yao W, Wen J, Cheng S. Real-time coordinated scheduling for ADNs with soft open points and charging stations. IEEE Trans Power Syst 2021; 36(6):5486–99.
[3] Denmark close to record wind output in 2020. <https://renews.biz/65510/denmark-close-to-wind-output-record-in-2020/>.
[4] Zhang M, Wu Q, Wen J, Lin Z, Fang F, Chen Q. Optimal operation of integrated electricity and heat system: A review of modeling and solution methods. Renew Sustain Energy Rev 2021;135:110098. https://doi.org/10.1016/j.rser.2020.110098.
[5] Bloess A, Schill W-P, Zerrahn A. Power-to-heat for renewable energy integration: a review of technologies, modeling approaches, and flexibility potentials. Appl Energy 2018;212:1611–26.
[6] Abu Dhabi, IRENA, Innovation landscape brief: Renewable power-to-heat, International Renewable Energy Agency, 2019.
[7] David A, Mathiesen BV, Averfalk H, Werner S, Lund H. Heat roadmap Europe: large-scale electric heat pumps in district heating systems. Energies 2017;10(4):578.
[8] Zhang M, Wu Q, Rasmussen T B H, Yang X, Wen J. Heat pumps in Denmark: Current situation of providing frequency control ancillary services. CSEE J Power Energy Syst 2021; early access.
[9] PlanEnergi, Oversigt over store el-drevne varmepumper, somproducerer varme til danske fjernvarmenet. https://planenergi.dk/wp-content/uploads/2017/08/Oversigt-over-store-varmepumper-aug-2017-BLP.pdf, 2017.
[10] Averfalk H, Ingvarsson P, Persson U, Gong M, Werner S. Large heat pumps in Swedish district heating systems. Renew Sustain Energy Rev 2017;79:1275–84.
[11] Denmark funds heat pumps for district heating, 2018. <https://dbdh.dk/2018/01/09/denmark-funds-heat-pumps-for-district-heating/>.
[12] EnergyLab Noardhavn Project. <http://www.energylabnordhavn.com/>.
[13] Energinet. Ancillary services from new technologies-Technical potentials and market integration. 2019.
[14] Zhang M, Fang J, Ai X, Zhou Bo, Yao W, Wu Q, et al. Partition-combine uncertainty set for robust unit commitment. IEEE Trans Power Syst 2020;35(4):3266–9.
[15] Zheng QP, Wang J, Liu AL. Stochastic optimization for unit commitment—a review. IEEE Trans Power Syst 2015;30(4):1913–24.
[16] Zhai Q, Guan X, Cheng J, Wu H. Fast identification of inactive security constraints in SCUC problems. IEEE Trans Power Syst 2010;25(4):1946–54.
[17] Liu X, Mancarella P. Modelling, assessment and Sankey diagrams of integrated electricity-heat-gas networks in multi-vector district energy systems. Appl Energy 2016;167:336–52.
[18] Zhang N, Lu Xi, McElroy MB, Nielsen CP, Chen X, Deng Yu, et al. Reducing curtailment of wind electricity in China by employing electric boilers for heat and pumped hydro for energy storage. Appl Energy 2016;184:987–94.
[19] Yao S, Gu W, Lu S, Zhou S, Wu Z, Pan G, et al. Dynamic optimal energy flow in the heat and electricity integrated energy system. IEEE Trans on Sustain Energy 2021; 12(1):179–90.
[20] Chen Z, Liu J, Liu X. GPU accelerated power flow calculation of integrated electricity and heat system with component-oriented modeling of district heating network. Appl Energy 2022;305:117832. https://doi.org/10.1016/j.apenergy.2021.117832.
[21] Chen X, McElroy MB, Kang C. Integrated energy systems for higher wind penetration in china: Formulation, implementation, and impacts. IEEE Trans Power Syst 2018;33(2):1309–19.
[22] Chen X, Kang C, O'Malley M, Xia Q, Bai J, Liu C, et al. Increasing the flexibility of combined heat and power for wind power integration in China: Modeling and implications. IEEE Trans Power Syst 2015;30(4):1848–57.
[23] Li Z, Wu W, Shahidehpour M, Wang J, Zhang B. Combined heat and power dispatch considering pipeline energy storage of district heating network. IEEE Trans Sustain Energy 2016;7(1):12–22.
[24] Wang D, Zhi Y-Q, Jia H-J, Hou K, Zhang S-x, Du W, et al. Optimal scheduling strategy of district integrated heat and power system with wind power and multiple energy stations considering thermal inertia of buildings under different heating regulation modes. Appl Energy 2019;240:341–58.
[25] Huang J, Li Z, Wu QH. Coordinated dispatch of electric power and district heating networks: A decentralized solution using optimality condition decomposition. Appl Energy 2017;206:1508–22.
[26] Zheng W, Hill DJ. Incentive-based coordination mechanism for distributed operation of integrated electricity and heat systems. Appl Energy 2021;285: 116373. https://doi.org/10.1016/j.apenergy.2020.116373.
[27] Ela E, Milligan M, Kirby B. Operating reserves and variable generation. National Renewable Energy Lab.(NREL), Golden, CO (United States), 2011.
[28] Energinet DK. Ancillary services to be delivered in Denmark Tender conditions. Technical report, Energinet, Fredericia 2012.
[29] Economics F. METIS Technical Note T4: Overview of European Electricity Markets. METIS Tech Notes 2016.
[30] Zhou H, Li Z, Zheng JH, Wu QH, Zhang H. Robust scheduling of integrated electricity and heating system hedging heating network uncertainties. IEEE Trans Smart Grid 2020;11(2):1543–55.
[31] You M, Wang Q, Sun H, Castro I, Jiang J. Digital twins based day-ahead integrated energy system scheduling under load and renewable energy uncertainties. Appl Energy 2022;305:117899. https://doi.org/10.1016/j.apenergy.2021.117899.
[32] Zhang M, Ai X, Fang J, Yao W, Zuo W, Chen Z, et al. A systematic approach for the joint dispatch of energy and reserve incorporating demand response. Appl Energy 2018;230:1279–91.
[33] Meesenburg W, Markussen WB, Ommen T, Elmegaard B. Optimizing control of two-stage ammonia heat pump for fast regulation of power uptake. Appl Energy 2020;271:115126. https://doi.org/10.1016/j.apenergy.2020.115126.
[34] Meesenburg W, Thingvad A, Elmegaard B, Marinelli M. Combined provision of primary frequency regulation from Vehicle-to-Grid (V2G) capable electric vehicles and community-scale heat pump. Sustain Energy Grids Netw 2020;23:100382. https://doi.org/10.1016/j.segan.2020.100382.
[35] Nielsen MG, Morales JM, Zugno M, Pedersen TE, Madsen H. Economic valuation of heat pumps and electric boilers in the Danish energy system. Appl Energy 2016; 167:189–200.
[36] Zhang M, Wu Q, Wen J, Pan Bo, Qi S. Two-stage stochastic optimal operation of integrated electricity and heat system considering reserve of flexible devices and spatial-temporal correlation of wind power. Appl Energy 2020;275:115357. https://doi.org/10.1016/j.apenergy.2020.115357.
[37] Tan J, Wu Q, Hu Q, Wei W, Liu F. Adaptive robust energy and reserve co-optimization of integrated electricity and heating system considering wind uncertainty. Appl Energy 2020;260:114230. https://doi.org/10.1016/j.apenergy.2019.114230.
[38] Tan J, Wu Q, Zhang M, Wei W, Liu F, Pan Bo. Chance-constrained energy and multi-type reserves scheduling exploiting flexibility from combined power and heat units and heat pumps. Energy 2021;233:121176. https://doi.org/10.1016/j.energy.2021.121176.
[39] Zhang M, Wu Q, Wen J, Xue X, Lin Z, Fang F. Real-time optimal operation of integrated electricity and heat system considering reserve provision of large-scale heat pumps. Energy 2021;237:121606. https://doi.org/10.1016/j.energy.2021.121606.
[40] Ding T, Wu Z, Lv J, Bie Z, Zhang X. Robust co-optimization to energy and ancillary service joint dispatch considering wind power uncertainties in real-time electricity markets. IEEE Trans Sustain Energy 2016;7(4):1547–57.
[41] Ding T, Qu M, Bai J, Jia W, Wu J, He Y, et al. Fast identifying redundant security constraints in SCUC in the presence of uncertainties. IET Gener Transm Dis 2020; 14(13):2441–9.
[42] Ma Z, Zhong H, Xia Q, Kang C, Wang Q, Cao X. An efficient method for identifying the inactive transmission constraints in network-constrained unit commitment. CSEE J Power Energy 2020. early access.
[43] IEEE-118 bus system data. <http://motor. ece.iit.edu/ Data/ 118bus ro.xls.>.
[44] Elia Grid data. <.>.
[45] The value of lost load. 2018. <https://www.tse-fr.eu/value-lost-load>.
[46] Bird L, Lew D, Milligan M, Carlini EM, Estanqueiro A, Flynn D, et al. Wind and solar energy curtailment: A review of international experience. Renew Sustain Energy Rev 2016;65:577–86.
[47] Zakariazadeh A, Jadid S, Siano P. Stochastic multi-objective operational planning of smart distribution systems considering demand response programs. Electr Power Syst Res 2014;111:156–68.
[48] Morales JM, Conejo AJ, Madsen H, Pinson P, Zugno M. Integrating renewables in electricity markets operational problems. Springer Science & Business Media; 2013.